Subcontract NP-1

WANL-TME-1713

21 November 1967

Westinghouse Astronuclear Laboratory

REACTIVITY PREDICTION AND REACTIVITY SHIMMING SPECIFICATION FOR THE NRX-A6 REACTOR

(Title Unclassified)

CONFIDENTIAL
RESTRICTED DATA
Atomic Energy Act - 1954

DECLASSIFIED

DISCLAIMER

~~CONFIDENTIAL~~
~~RESTRICTED DATA~~
~~Atomic Energy Act - 1954~~

DECLASSIFIED

MASTER

Subcontract NP-1

WANL-TME-1713

21 November 1967

Westinghouse Astronuclear Laboratory

REACTIVITY PREDICTION AND REACTIVITY SHIMMING SPECIFICATION FOR THE NRX-A6 REACTOR

(Title Unclassified)

DISTRIBUTION OF THIS DOCUMENT UNLIMITED

PREPARED BY: D. J. Hill
C. Seibert
E. Iwinski

Analysis Done By:

D. J. Hill
P. J. Sipush
L. I. Ortenberg
C. Seibert
E. Iwinski

INFORMATION CATEGORY
C - D
AUTHORIZED CLASSIFIER DATE 2/16/67

Exempt from CCRP Re-review Requirements
(per 7/22/82 Duff/Caudle memorandum)

Classification cancelled (or changed to _____)
by authority of TID-1400-S2
by DJ Dempsey DTIE, date 7-14-75

DECLASSIFIED

~~CONFIDENTIAL~~
~~RESTRICTED DATA~~
~~Atomic Energy Act - 1954~~

ACKNOWLEDGEMENT

Acknowledgement is given to WNCO Quality Engineering, WANL Reactor Assembly, WNCO Data Systems, and WANEF for the assistance rendered in obtaining component weights and reactivity coefficients used in the determination of the NRX-A6 shim content. In addition to the major contributors to the NRX-A6 reactivity estimate, W. Freidhof, R. Rittenberger, S. Salah, D. G. Bevard, A. L. Mowery and D. Mangan also aided in the analysis.

Astronuclear Laboratory

WANL-TME-1713

ABSTRACT

The reactivity of the NRX-A6 reactor was calculated relative to the PAX-El reactor at WANEF, which incorporated the NRX-A6 reflector rings and control drums. In determining the relative reactivities of NRX-A6 and PAX-El, the core material inventories for the two reactors were determined with the Automated Materials Data System (AMDS) computer program (Reference 1). The non-core material inventories were based on the measured masses of the individual components involved. The reactivity difference between the NRX-A6 and PAX-El fuel was determined by (a) experimentally measuring the reactivity change which occurred when NRX-A6 preproduction fuel was substituted for a quadrant of PAX-El fuel, (b) multiplying this reactivity change by a calculated factor which was approximately four, and (c) correcting the results for quadrant interaction effects. Where applicable, core reactivity changes were taken to be the product of the mass difference and the appropriate reactivity coefficient at the location of the element. The mass differences were determined on an element-by-element basis. The reactivity coefficients were determined by interpolation of radial reactivity coefficient curves. The reactivity differences for non-core materials were also calculated for the most part by applying reactivity coefficients to measured mass differences.

THIS PAGE

WAS INTENTIONALLY

LEFT BLANK

TABLE OF CONTENTS

		Page
ABSTRACT		i
ACKNOWLEDGEMENT		ii
TABLE OF CONTENTS		iii
LIST OF ILLUSTRATIONS		iv
1.0 (CRD)	INTRODUCTION	1
2.0 (CRD)	CONCLUSIONS	4
3.0 (CRD)	METHOD OF ANALYSING THE NRX-A6 REACTIVITY BASED ON A NON-SYMMETRIC EXPERIMENTAL CONFIGURATION	6
4.0 (CRD)	NRX-A6 AND PAX-E1 MASSES	17
	4.1 Definition of Reactor Regions	17
	4.2 Determination of Reactor Masses	17
	4.2.1 Core Region	20
	4.2.2 Regions Outside the Core	25
	4.3 Uncertainties in Reactor Masses	32
5.0 (CRD)	REACTIVITIES AND REACTIVITY COEFFICIENTS	34
	5.1 Core Reactivity Coefficients	39
	5.2 Fuel Interchange Experiment	50
	5.3 Non-Core Reactivity Coefficients	50
	5.4 Uncertainties in Reactivity Effects	54
6.0 (CRD)	NRX-A6/PAX-E1 CORE REACTIVITY DIFFERENCES	57
	6.1 Fuel Differences	57
	6.1.1 Method of Extrapolating Test Quadrant Data to a Full Core	59
	6.1.2 Reactivity Differences Between PAX-E1 Test Quadrant Extrapolation and PAX-E1 Fuel	66

TABLE OF CONTENTS (Cont'd.)

			Page
	6.1.3	Reactivity Difference Between the NRX-A6 Test Quadrant Extrapolation and the PAX-El Test Quadrant Extrapolation Fuel	67
	6.1.4	Reactivity Difference Between NRX-A6 Test Quadrant Extrapolation and NRX-A6 Fuel	71
	6.1.5	Summary of the Reactivity Differences Between the NRX-A6 and PAX-El Fuel	71
6.2		NRX-A6/PAX-El Non-Fuel Differences	73
	6.2.1	Central Support Elements	73
	6.2.2	Instrumentation	76
	6.2.3	Core Hardware	78
6.3		Summary of NRX-A6 and PAX-El Core Reactivity Differences	79
7.0 (CRD)		NRX-A6/PAX-El NON-CORE REACTIVITY DIFFERENCES	80
7.1		Filler Strip and Lateral Support Region Differences	80
7.2		Beryllium Reflector Differences	83
7.3		Support Block Differences	84
7.4		Cluster Plate and Support Plate Differences	84
8.0 (CRD)		ADDITIONAL REACTIVITY EFFECTS WHICH OCCURRED BETWEEN NRX-A6 AND PAX-El	86
8.1		Reactivity Effect of Instrumentation	86
8.2		Reactivity Effect of External Structures	88
8.3		Reactivity Effect of Bundling Pressure	90
8.4		Reactivity Effect of Pressure Vessel	90

TABLE OF CONTENTS (Cont'd.)

		Page
9.0 (CRD)	UNCERTAINTIES IN THE NRX-A6 REACTIVITY ESTIMATE	93
10.0 (CRD)	DETERMINATION OF THE NRX-A6 NEGATIVE SHIMMING	96
	10.1 Selection of the NRX-A6 Aim Cold Critical Drum Position	96
	10.2 Summary of the NRX-A6 and PAX-El Reactivity Comparison	98
	10.3 Selection of NRX-A6 Shim Content	98
11.0 (U)	REFERENCES	100

THIS PAGE

WAS INTENTIONALLY

LEFT BLANK

LIST OF ILLUSTRATIONS

Figure No.		Page
2.1	NRX-A6 Shimming Distribution and Instrumentation Summary	5
3.1	Nomenclature for Fuel Inventories and Fuel Reactivity Effects	7
3.2	Reference Reactor for NRX-A6/PAX-El Reactivity Estimate	8
3.3	PAX-El Configuration Before and After the Fuel Substitution Experiment	9
3.4	Conceptual Reactor Configuration in Obtaining the Reactivity Difference Between the NRX-A6 and PAX-El Fuel	11
4.1	Region Identification and Volumes	18
4.2	PAX-El, Number of Components Within the Core by Radial Region	21
4.3	NRX-A6, Number of Components Within Core by Radial Region	22
4.4	PAX-Q, Number of Components Within the Core by Radial Region	23
4.5	A6-Q, Number of Components Within the Core by Radial Region	24
4.6	PAX-El, Material Masses by Radial Region	26
4.7	NRX-A6, Material Masses by Radial Region	27
4.8	PAX-Q, Material Masses by Radial Region	28
4.9	A6-Q, Material Masses by Radial Region	29
4.10	PAX-El Reflector Region Masses	30
4.11	NRX-A6 Reflector Region Masses	31

LIST OF ILLUSTRATIONS (Cont'd.)

Figure No.		Page
4.12	Reactivity Uncertainty Due to Mass Uncertainties	33
5.1	PAX-EO Reactor Configuration	35
5.2	PAX-E1 Reactor Configuration	37
5.3	PAX-E2 Reactor Configuration	38
5.4	Carbon Reactivity Coefficient as a Function of Radial Position	40
5.5	Uranium Reactivity Coefficient as a Function of Radial Position	41
5.6	Niobium Reactivity Coefficient as a Function of Radial Position	42
5.7	Molybdenum Reactivity Coefficient as a Function of Radial Position	43
5.8	Tantalum Reactivity Coefficient as a Function of Radial Position	44
5.9	Molybdenum Reactivity Coefficient as a Function of Wire Diameter	45
5.10	Niobium Reactivity Coefficient as a Function of Wire Diameter	46
5.11	Average Reactivity Coefficients for Core Regions	47
5.12	A6-Q/PAX-Q Fuel Interchange Experimental Results	51
5.13	Average Reactivity Coefficient for Non-Core Regions	53
5.14	Reactivity Uncertainty Due to Reactivity Effect Uncertainties	55
6.1	Relative Worth of PAX-Q Fuel Extrapolated to a Full Core	60

LIST OF ILLUSTRATIONS (Cont'd.)

Figure No.		Page
6.2	Relative Worth of A6-Q Fuel Extrapolated to a Full Core	61
6.3	Reactivity Comparison Between PAX-El and PAX-QE Fuel	62
6.4	Reactivity Comparison Between A6-Q and PAX-Q Fuel	63
6.5	Reactivity Comparison Between A6-QE and PAX-QE Fuel	64
6.6	Reactivity Difference Between A6-QE and PAX-QE Fuel Based on the Fuel Interchange Experiment	68
6.7	Reactivity Difference Between NRX-A6 and A6-QE Fuel	72
6.8	Summary of the Reactivity Differences Between NRX-A6 and PAX-El Fuel	74
6.9	NRX-A6/PAX-El Core Reactivity Differences	75
6.10	Reactivity Worth of Core Instrumentation	77
7.1	NRX-A6/PAX-El Non-Core Reactivity Differences	81
8.1	Reactivity Worth of Non-Core Instrumentation	87
8.2	Reactivity Effect of Radial Bundling on Reactivity	91
9.1	Experience in Reactivity Shimming Previous NRX Reactors	94
10.1	NRX-A6 Operating Reactivity Changes	97
10.2	Summary of NRX-A6 and PAX-El Reactivity Differences	99

SECTION 1.0

(CRD) INTRODUCTION

Analysis of the expected corrosion behavior of the NRX-A6 fuel during hot firing indicated that an orifice angle of 105° and a critical drum position at the hot start-of-life of 90° would be desirable. The initial analysis of the expected cold-to-hot operating reactivity change indicated a net reactivity loss, in going to full power conditions, of 0.13$. Therefore, an aim ambient delayed critical drum position of 88° was chosen in order to obtain the desired hot critical drum position of 90°.

The reactivity of the NRX-A6 reactor was determined in a manner which is essentially different from that which was used for previous NRX reactors. Like previous NRX reactors, the NRX-A6 reactivity estimate was based on a preceding reactor; however, for previous NRX reactors, this estimate was essentially determined by taking the product of a mass difference between the two reactors and an appropriate reactivity coefficient. A similar procedure was used for the NRX-A6/PAX-E1 reactivity comparison for unfueled elements, core hardware, and non-core components; however, the reactivity difference between the NRX-A6 and PAX-E1 fuel was based primarily on the experimentally measured reactivity change which occurred when NRX-A6 preproduction fuel was substituted for a quadrant of PAX-E1 fuel.

The NRX-A6 reactor is considerably different neutronically from previous NRX reactors. Consequently, the PAX reactor was modified to simulate the NRX-A6 reactor configuration. This NRX-A6 configuration of PAX is identified as the PAX-E1 reactor.

The PAX-E1 reactor had an ambient delayed critical drum position of 87.7° in the following configuration:

1. The reactor contained one tantalum carbide negative shim worth 6.3¢ in reactivity.
2. The center of the PAX-E1 core contained 54 loading code 89 fuel elements from the NRX-A3 production which were used to simulate NRX-A6 loading code 18 fuel because sufficient quantity of this fuel was not available.
3. The remainder of the PAX-E1 core consisted of fuel from NRX-A2 production interspersed with unfueled nineteen-hole graphite to simulate the NRX-A6 uranium loading distribution by the replacement of fueled elements. These unfueled elements are identified as code 04 elements. Because of the code 04 elements, the PAX-E1 fuel was more heterogeneous in nature than the NRX-A6 fuel.
4. The PAX-E1 reactor contained mockups of the NRX-A6 filler strip and lateral support region.
5. The PAX-E1 reactor contained the actual NRX-A6 beryllium reflector rings and control drums; however, the reflector did not contain the NRX-A6 lateral support hardware other than the Inconel springs.

This report is organized in the following manner:

Section 3.0 describes in general terms the method by which the reactivity difference between the NRX-A6 and PAX-E1 fuel is determined. The

details of the fuel reactivity calculations are given in Section 6.0 along with results for the other components in the core.

Section 4.0 describes the manner in which the material inventories for the NRX-A6 and PAX-E1 reactors were obtained. The actual inventories and the reactivity uncertainty due to inventory uncertainties are also contained in the section.

Section 5.0 gives the core reactivity coefficients, the non-core reactivity coefficients, and the fuel interchange results used in the NRX-A6/PAX-E1 reactivity comparison. This section also includes the reactivity uncertainty due to reactivity effects uncertainties.

Sections 7.0 and 8.0 describe the non-core reactivity differences between the NRX-A6 and PAX-E1 and the method by which these effects were obtained.

Section 9.0 summarizes the uncertainties in the NRX-A6 reactivity estimate and give the experience to date for reactivity shimming previous NRX reactors.

Section 10.0 describes the criteria for selecting the NRX-A6 aim critical drum position. This section also summarizes the NRX-A6/PAX-E1 reactivity comparison and gives the criteria for determining the negative shim pattern in the NRX-A6.

SECTION 2.0

(CRD) CONCLUSIONS

The NRX-A6 reactivity analysis indicated that, in order to obtain the desired ambient delayed critical drum position of 88°, the NRX-A6 reactor would require 1.62$ worth of negative shims. Figure 2.1 shows the position of the 38 TaC-loaded central support elements required for the insertion of this amount of negative reactivity.

The NRX-A6 reactor is predicted to have an ambient delayed critical drum position of 87.4° with a 2 σ uncertainty of $\pm$10°. This uncertainty was derived by considering the performance in predicting the critical drum position of previous NRX reactors and the added uncertainties which are inherent in the NRX-A6 method of reactivity analysis.

Astronuclear Laboratory

FIGURE 2.1
NRX-A6 SHIMMING DISTRIBUTION
AND INSTRUMENTATION SUMMARY

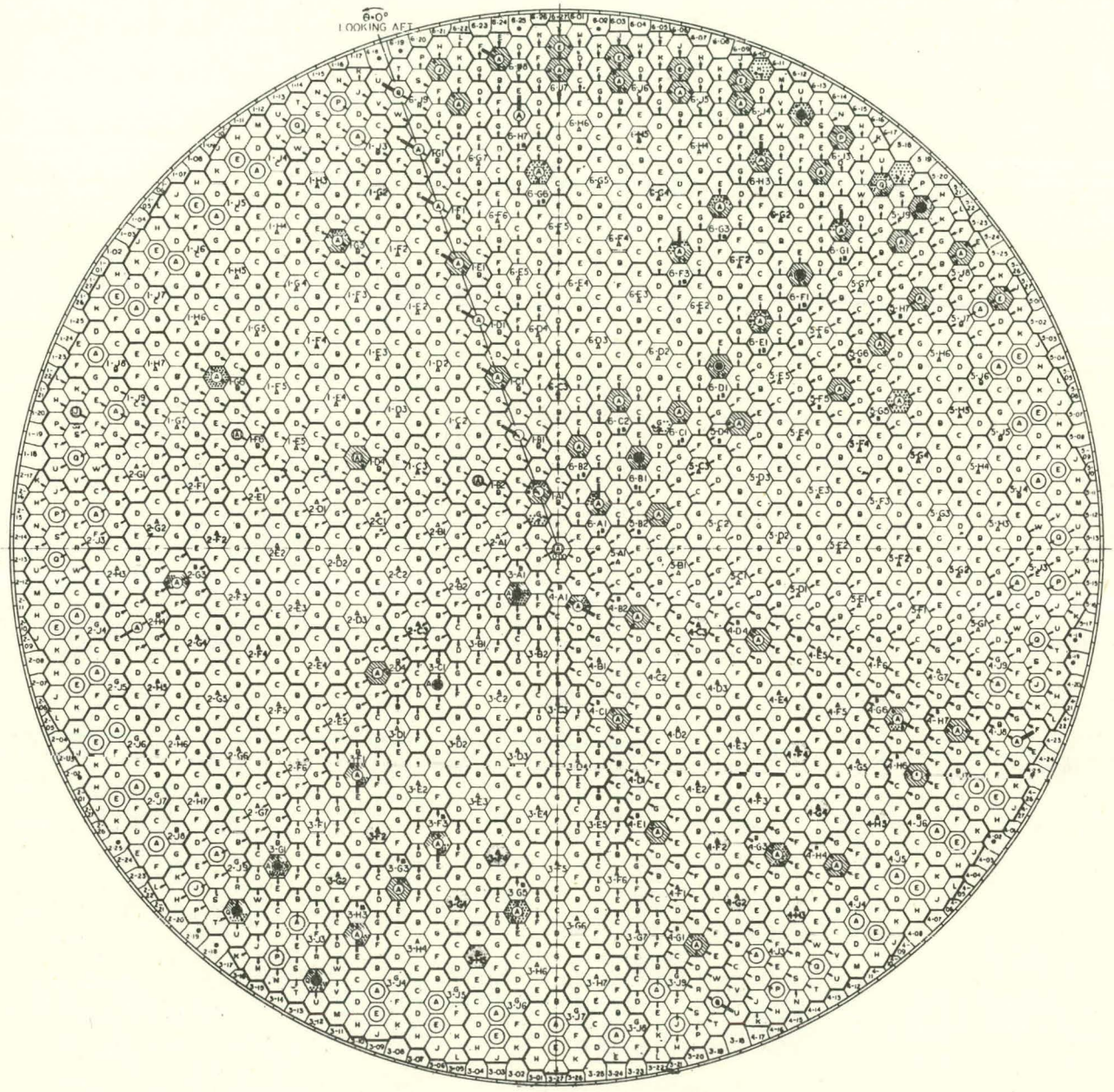

SECTION 3.0

(CRD) METHOD OF ANALYZING THE NRX-A6 REACTIVITY BASED ON A NON-SYMMETRIC EXPERIMENTAL CONFIGURATION

The following section is a general description of the method by which the reactivity difference between the NRX-A6 and PAX-El fuel was determined. The results of the calculational technique described here are given in Section 6.1

Figure 3.1 defines the nomenclature used in discussing the reactivity change between NRX-A6 and PAX-El. Figure 3.2 shows the initial PAX-El reactor configuration as described in Section 1.0. Figure 3.3 shows the PAX-El core configuration before and after the fuel substitution experiment.

Before the fuel substitution experiment, the PAX-El core consisted of the code 89 fuel (A3-C fuel) at the center or keyhole region of the core. The fuel outside the keyhole region contained 270° of the PAX-El fuel and 90° of PAX-El fuel which would be involved in the fuel substitution experiment. The fuel in this 90° section is defined symbolically as PAX-Q fuel. After the fuel substitution, the fuel in the PAX-El core consisted of the A3-C fuel at the center of the core, 270° of PAX-El fuel, and 90° of NRX-A6 preproduction fuel which is defined symbolically as A6-Q fuel.

The problem of determining the reactivity of the NRX-A6 fuel relative to the PAX-El fuel now becomes one of using the results obtained in the quadrant fuel substitution experiment and extrapolating to a full core

FIGURE 3.1

NOMENCLATURE FOR FUEL INVENTORIES

AND FUEL REACTIVITY EFFECTS

Term	Definition
PAX-E1	Refers to the complete, 360° PAX-E1 core which consisted of fuel produced for the NRX-A2 reactor. The uranium distribution in the PAX-E1 fuel was made similar to that in NRX-A6 by the replacement of fueled elements with nineteen-holed unfueled elements.
PAX-Q	Refers to the PAX-E1 fuel in the test quadrant (90°) in which the fuel substitution experiment occurred.
PAX-QE	Refers to the reactivity effect of PAX-Q fuel which has been extrapolated to a complete core (360°).
A6-Q	Refers to the quadrant of NRX-A6 preproduction fuel (90°) which was involved in the fuel substitution experiment.
A6-QE	Refers to the reactivity effect of the A6-Q fuel which has been extrapolated to a complete core (360°).
NRX-A6	Refers to the complete, (360°) NRX-A6 core.
A3-C	Refers to the 54, NRX-A3 code 89, elements which were in the keyhole or center of the PAX-E1 core. These elements were placed in PAX-E1 because sufficient A6-Q code 18 elements were not available, and the uranium content of this fuel was similar to the A6-Q code 18 elements.

FIGURE 3.2

REFERENCE REACTOR FOR NRX-A6/PAX-E1 REACTIVITY ESTIMATE

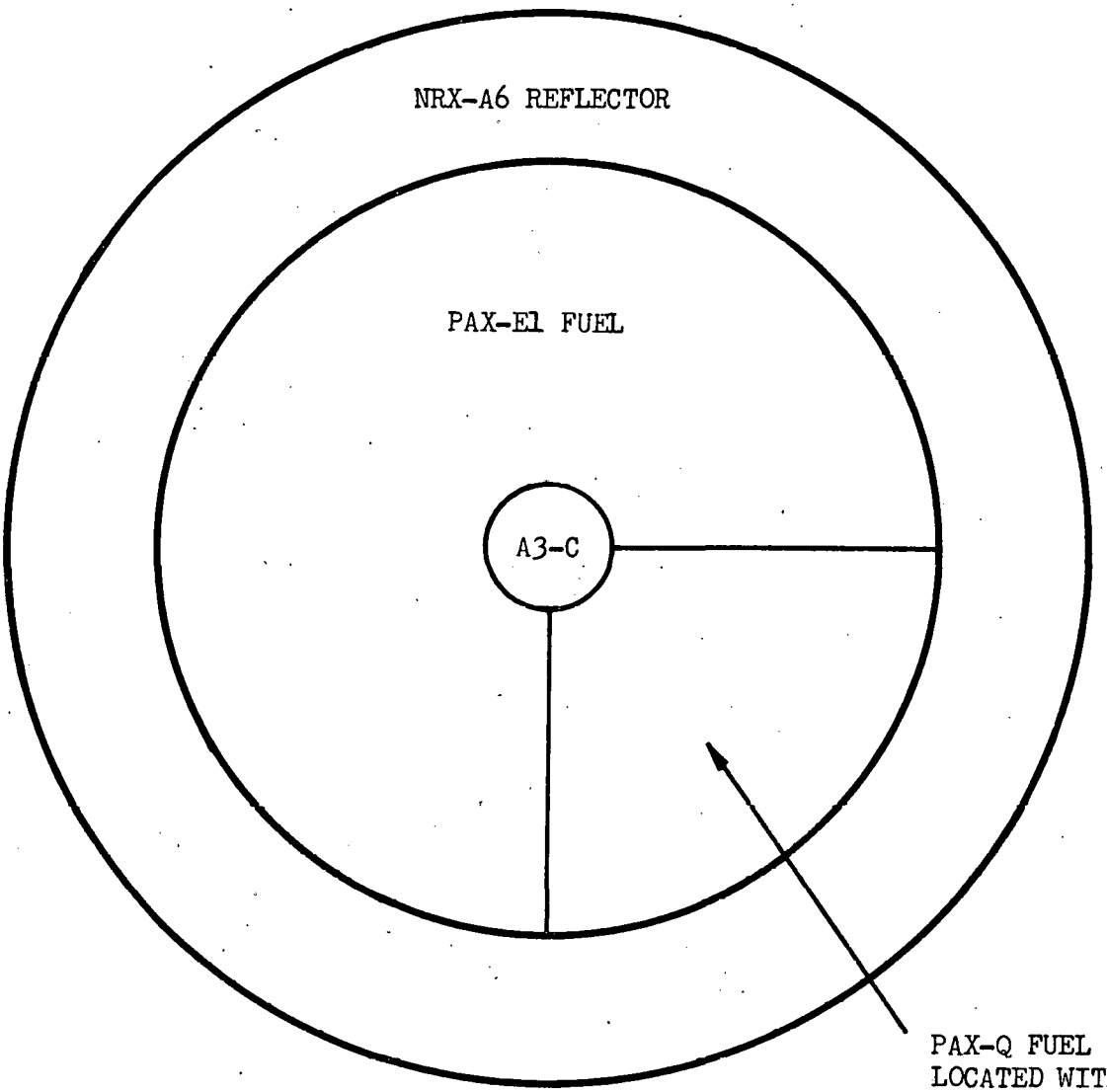

Astronuclear Laboratory

FIGURE 3.3

PAX-E1 CONFIGURATION BEFORE AND AFTER THE FUEL SUBSTITUTION EXPERIMENT

PAX-E1
BEFORE FUEL SUBSTITUTION

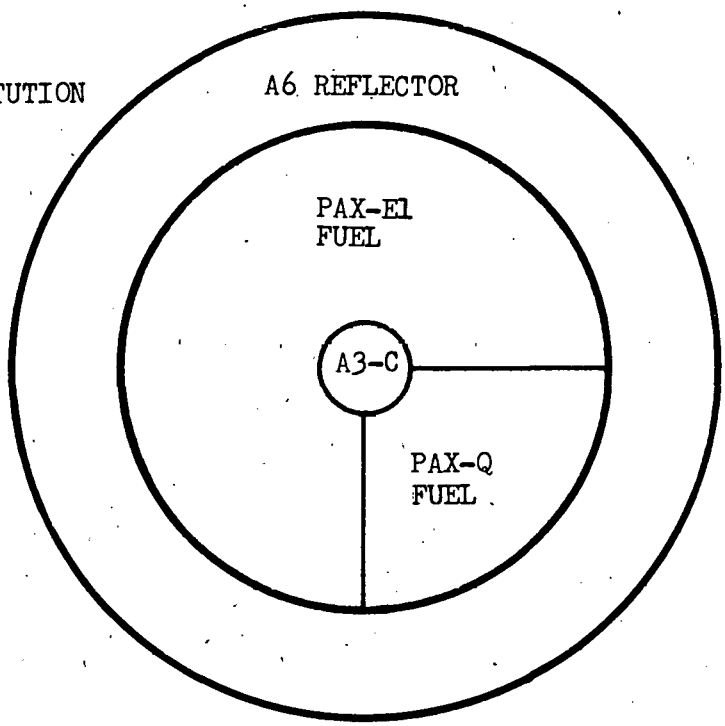

PAX-E1
AFTER FUEL SUBSTITUTION

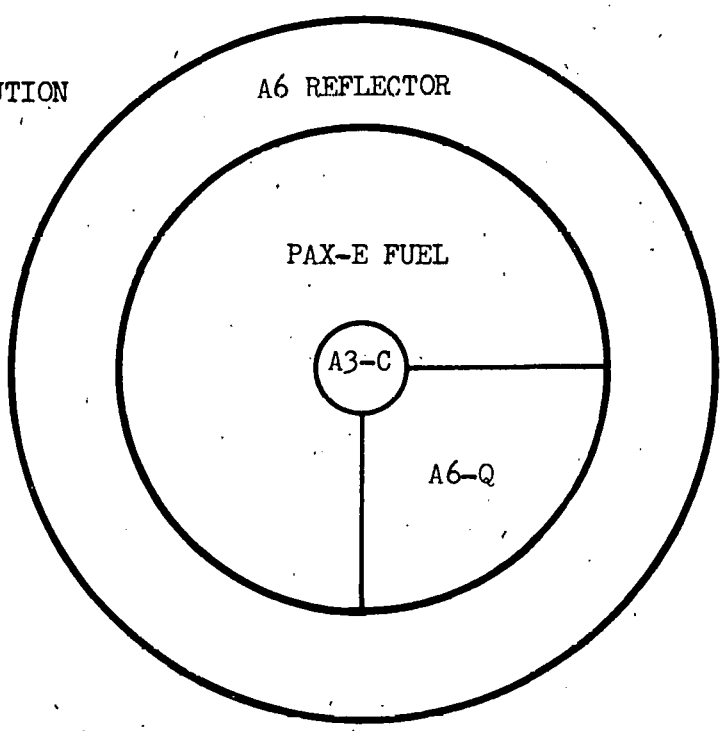

(360°) of fuel. Figure 3.4 shows the conceptual reactor configuration associated with the following steps involved in obtaining the reactivity difference between the NRX-A6 and PAX-E1 fuel.

Step 1 The first reactor configuration is the initial PAX-E1 core which, has been previously described.

Step 2 The second reactor configuration, which is conceptual, consists of the A3-C fuel at the center of the core, while the remaining fuel is the PAX-Q fuel which has been extrapolated to a complete core (360°) of fuel. This fuel outside the A3-C fuel is designated as PAX-QE fuel. The exact method of extrapolating the PAX-Q fuel to the PAX-QE fuel is described in Section 6.1. The reactivity difference between the PAX-QE fuel and the PAX-E1 fuel is taken to be the product of the mass differences between the two sets of fuel and the appropriate reactivity coefficients.

Step 3 The third reactor configuration, which is conceptual, consists of the A3-C fuel at the center of the core with the remaining portion of the fuel being A6-Q fuel which has been extrapolated to a complete core (360°) of fuel. This fuel outside the A3-C fuel is designated as A6-QE fuel. Again, the exact means for extrapolating the A6-Q fuel to the A6-QE is described in Section 6.1. The method of determining the reactivity difference between

FIGURE 3.4

CONCEPTUAL REACTOR CONFIGURATIONS IN OBTAINING THE REACTIVITY DIFFERENCE BETWEEN THE NRX-A6 AND PAX-E1 FUEL

STEP 1

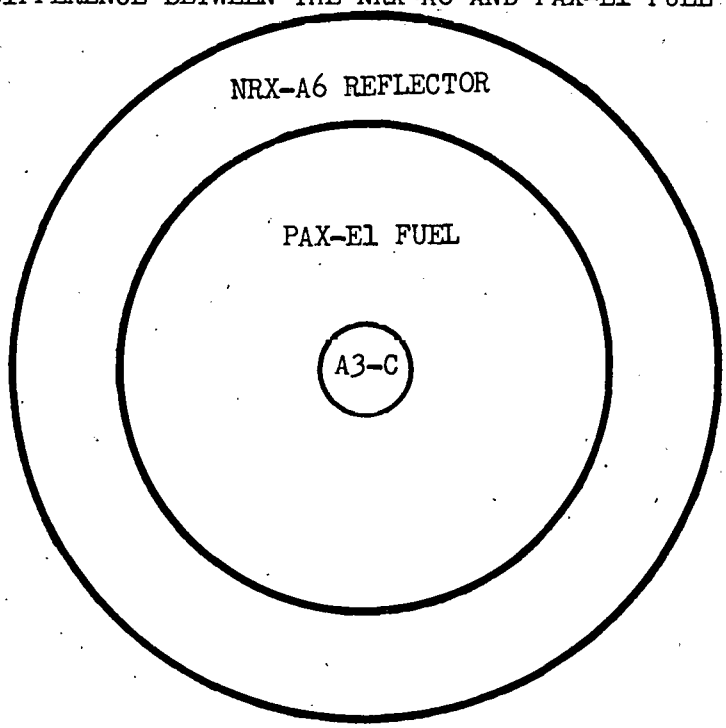

STEP 2

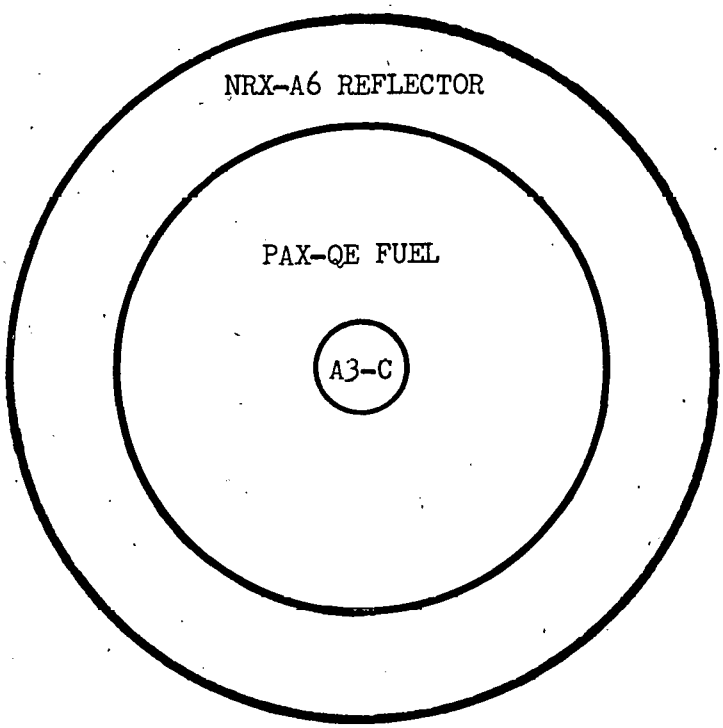

FIGURE 3.4 (Cont'd.)

STEP 3

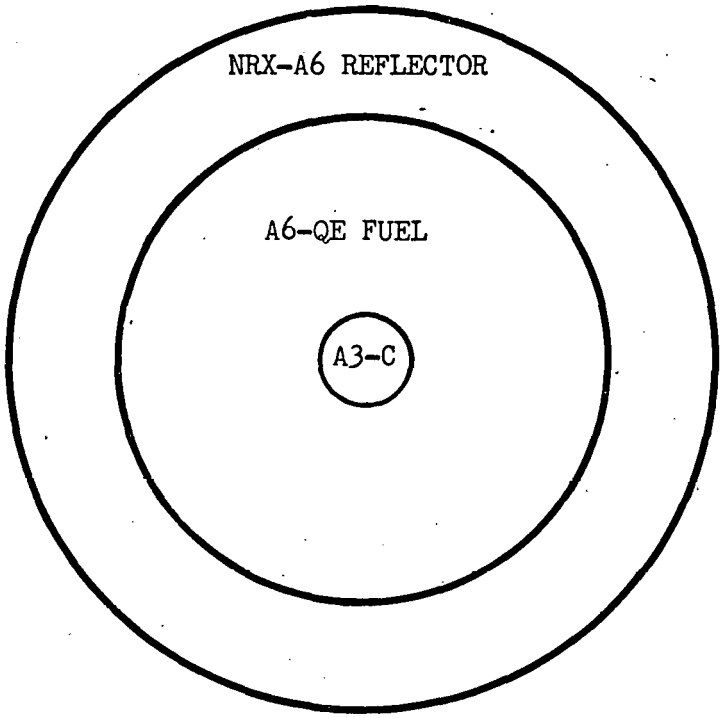

STEP 4

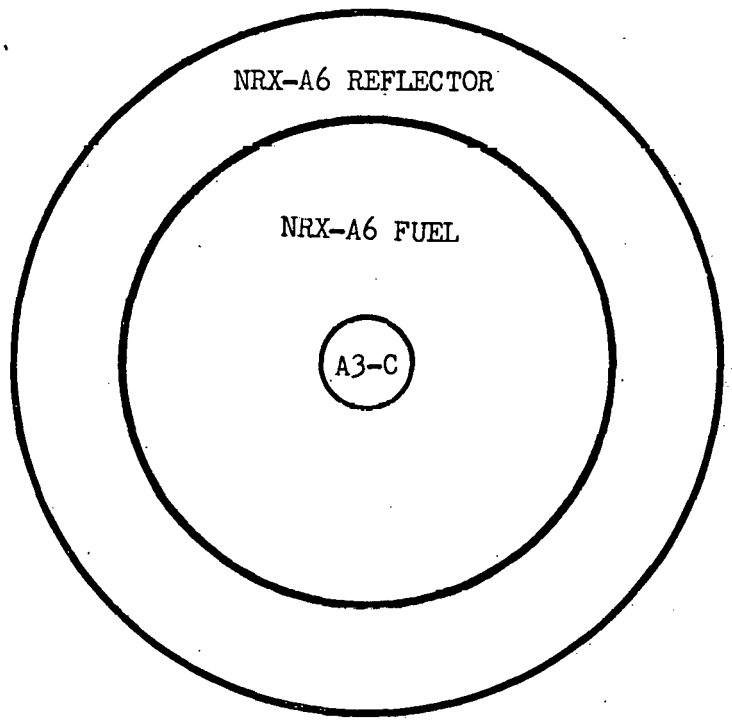

FIGURE 3.4 (Cont'd.)

STEP 5

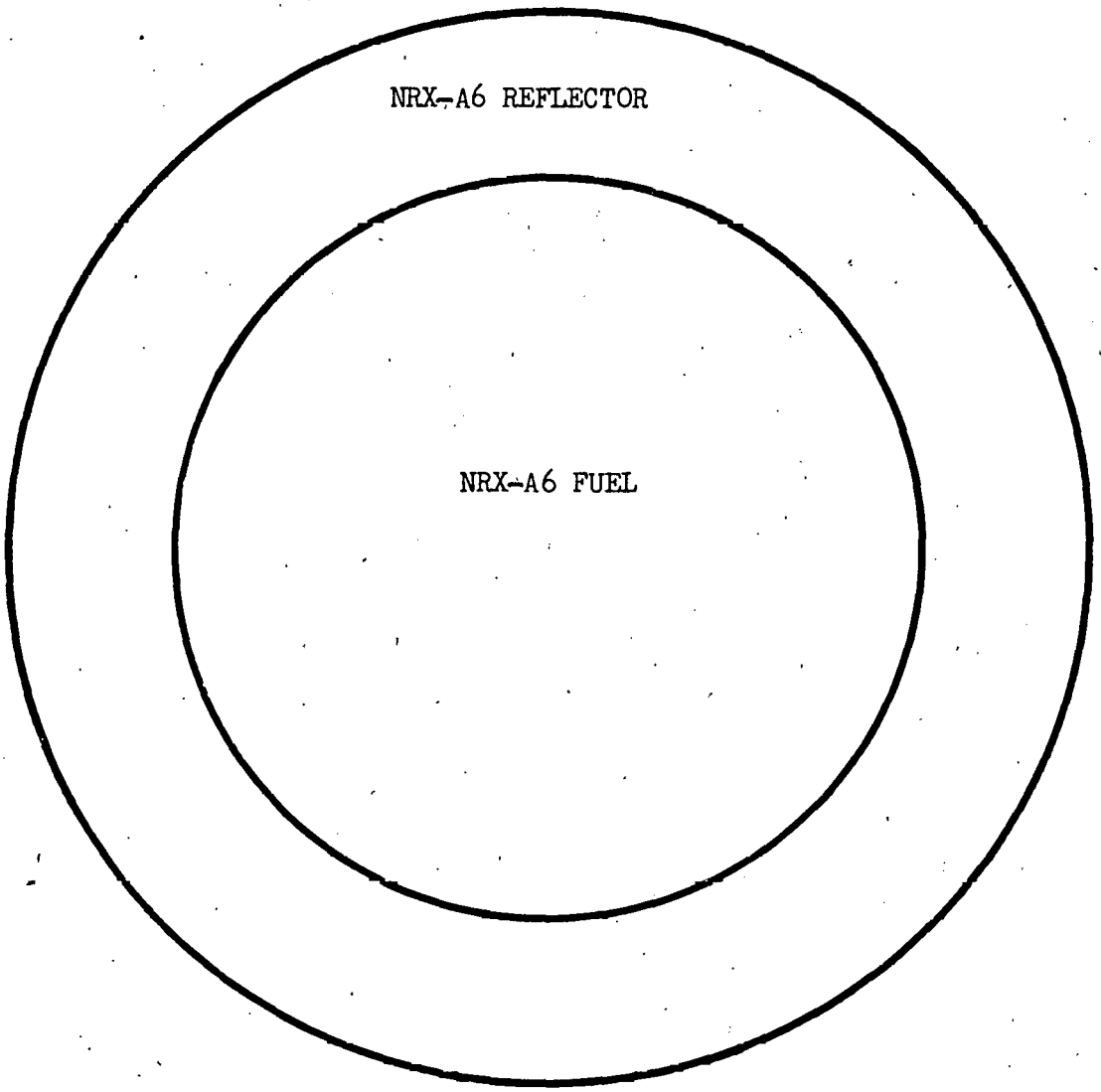

the A6-QE fuel and the PAX-QE fuel is given by the following formula:

$$\rho\,(\text{A6-QE/PAX-QE}) = \Delta\rho \times \frac{\rho\,(\text{A6-QE/PAX-QE})^{\text{Calc.}}}{\rho\,(\text{A6-Q/PAX-Q})^{\text{Calc.}}}$$

where,

$\rho\,(\text{A6-QE/PAX-QE})$ = the reactivity difference between the A6-QE and PAX-QE fuel in cents.

$\Delta\rho$ = the experimentally measured reactivity difference between the A6-Q fuel and the PAX-Q fuel.

$\rho\,(\text{A6-QE/PAX-QE})^{\text{Calc.}}$ = the reactivity change between the A6-QE fuel and the PAX-QE fuel in cents calculated from mass differences and reactivity coefficients.

$\rho\,(\text{A6-Q/PAX-Q})^{\text{Calc.}}$ = the reactivity change between the A6-Q fuel and the PAX-Q fuel in cents calculated from mass differences and reactivity coefficients.

This formula assumes that any error in the calculated reactivity changes are multiplicative in nature; therefore, any error in the calculated reactivity change will cancel when the ratio of the reactivity differences of the A6-QE/PAX-QE fuel to the A6-Q/PAX-Q fuel is determined. Another correction is applied to the result obtained from the preceding formula to account for interaction effects between the A6-Q fuel and

the remaining 270° of PAX-E1 fuel. The details of this correction are given in Section 6.1.

Step 4 The fourth reactor configuration, which is conceptual, consists of the A3-C fuel at the center of the core with the remaining portion of the fuel being the actual NRX-A6 fuel. The reactivity difference between the NRX-A6 fuel and the A6-QE fuel is taken to be the product of the mass differences between the two sets of fuel and the appropriate reactivity coefficients.

Step 5 The fifth and final reactor configuration consists of a complete core of NRX-A6 fuel. The only change between this reactor configuration and the previous one is that the A3-C fuel has been replaced by NRX-A6 fuel. The reactivity difference between the A3-C fuel and the NRX-A6 in the center of the core was obtained by multiplying the mass differences by the appropriate reactivity coefficients.

The reactivity difference between the NRX-A6 fuel and the PAX-E1 fuel is now given by the following formula:

$$\rho(\text{NRX-A6/PAX-E1}) = \rho(\text{PAX-QE/PAX-E1}) + \rho(\text{A6-QE/PAX-QE}) + \rho(\text{NRX-A6/A6-QE}) + \rho(\text{NRX-A6/A3-C})$$

where,

ρ(PAX-QE/PAX-E1) = the reactivity difference between the PAX-QE and the PAX-E1 fuel (Step 1 and Step 2).

ρ (A6-QE/PAX-QE) = the reactivity difference between the A6-QE and the PAX-QE fuel (Step 2 and Step 3).

ρ (NRX-A6/A6-QE) = the reactivity difference between the NRX-A6 and the A6-QE fuel (Step 3 and Step 4).

ρ (NRX-A6/A3-C) = the reactivity difference between the NRX-A6 fuel at the center of the core and the A3-C fuel (Step 4 and Step 5).

The preceding method of determining the reactivity difference between the NRX-A6 and PAX-E1 fuel eliminates some of the problems which have occurred in determining the fuel reactivity differences for previous NRX reactors. The major problem eliminated by this technique is that of a discrepancy or bias in the nondestructive testing technique for determining the inventory of the fuel; however, several effects which had not been present in the fuel reactivity estimates of previous NRX reactors now occur. These effects are as follows:

1. interaction effects in the fuel substitution experiment, and
2. the effects of the PAX-E1 fuel heterogeneity on the reactivity worth of core materials and reflector materials.

SECTION 4.0

(CRD) NRX-A6 AND PAX-E1 MASSES

4.1 Definition of Reactor Regions

The core regions of NRX-A6 and PAX-E1 were divided into nine subregions so that a more accurate estimate of the reactivity differences between the two reactors could be made. Subregion descriptions in the A6-Q and PAX-Q test quadrants were the same as those used in NRX-A6 and PAX-E1. The regions used in the comparisons are as follows:

Core Region	Outer Radius, cm
1	15.747
2	20.445
3	25.391
4	32.491
5	34.294
6	36.689
7	39.480
8	41.719
9	43.804

Table 4.1 describes the regions used in each reactor in detail.

4.2 Determination of Reactor Masses

The measured masses of components were used to compile the material inventories of NRX-A6 and PAX-E1 reactors and the A6-Q and PAX-Q quadrants. These masses were corrected to include only the material present

FIGURE 4.1
NRX-A6 AND PAX-E1
REGION IDENTIFICATION AND VOLUMES

RADIAL REGION (OUTER RADIUS GIVEN IN CM)

Region	Outer Radius, cm	Volume, cc
Core 1 NRX-A6 Fuel Loading Codes 18, 19 PAX-E1 Fuel Loading Codes 18, 99, 04	15.747	1.02892×10^5
Core 2 NRX-A6 Fuel Loading Codes 19, 20 PAX-E1 Fuel Loading Codes 99, 04	20.445	0.70552×10^5
Core 3 NRX-A6 Fuel Loading Codes 19, 20, 21 PAX-E1 Fuel Loading Code 99	25.391	0.94069×10^5
Core 4 NRX-A6Fuel Loading Codes 20, 21 PAX-E1 Fuel Loading Code 99	32.491	1.70525×10^5
Core 5 NRX-A6 Fuel Loading Codes 19, 20, 21 PAX-El Fuel Loading Code 99	34.294	0.49964×10^5
Core 6 NRX-A6Fuel Loading Codes 16, 17, 18 PAX-E1 Fuel Loading Codes 99, 04	36.689	0.70542×10^5
Core 7 NRX-A6 Fuel Loading Codes 15, 16, 17 PAX-E1 Fuel Loading Codes 69, 79	39.480	0.88211×10^5
Core 8 89, 99, 04 NRX-A6Fuel Loading Codes 13, 14 PAX-El Fuel Loading Codes 49, 59,	41.719	0.75438×10^5
Core 9 69, 01 NRX-A6 Fuel Loading Codes 11, 12, 13 PAX-El Fuel Loading Codes 39, 49, 04	43.801	0.7399×10^5
Filler Strip	45.174	0.50581×10^5
Lateral Support	47.831	1.02539×10^5
Beryllium Reflector	62.814	6.87889×10^5
Void	63.183	0.19291×10^5
Pressure Vessel	64.884	0.90434×10^5

in the 52-inch long axial region bounded by planes at each end of the fueled elements. This method of determining material weights assumes that the reactivity of materials above and below this region is the same in both reactors. Because of the similarity between all of the components in the reactors, the error associated with this assumption is negligible.

The measured masses of some materials, for example niobium and molybdenum, were adjusted to the mass of material in a uniform axial distribution having an equal reactivity effect. This was accomplished by weighting the axial mass distribution of the material with a sine-squared function over a 52-inch length. This then gave an equivalent mass of material to which a reactivity coefficient determined for a uniform distribution of material in the core could be applied. A sine-squared weighting function was used because point values and integrated values over a portion of the length of the function could be easily determined, and because the sine-squared function closely approximates the axial reactivity profile (See Reference 2 for details).

The masses which were adjusted by sine-squared weighting for NRX-A6 and PAX-E1 are:

1) Mass of uranium in fuel elements.
2) Mass of niobium coating in fuel elements.
3) Mass of molybdenum coating in fuel elements.
4) Mass of materials in thermal capsules.
5) Mass of materials in thermocouples.
6) Mass of materials in thermometers.

7) Mass of material in filler tiles.

8) Mass of materials in impedance wrapper.

9) Mass of materials in friction plane.

10) Mass of materials in the inner and outer seal segments.

The application of a weighting function to these masses is equivalent to adjusting their reactivity coefficients by the same factor.

4.2.1 Core Region

The masses of the materials in the fueled and unfueled elements were compiled by means of the AMDS computer program (See Reference 1). Punched data cards specifying the total carbon, uranium, niobium and molybdenum masses for each element along with the niobium coating profile were obtained from the WNCO and the UCC ND Y-12 data systems. These cards were used as input to the AMDS program which sine-square weighted the amount of niobium in each element and summed the mass of each material in the elements. Representative masses for the other components in the core were measured to obtain the total core inventory due to them.

Fueled and unfueled element inventories, by core region, for PAX-E1 and NRX-A6 are shown in Figures 4.2 and 4.3, respectively. The element inventories for the PAX-Q and A6-Q quadrants are given in Figures 4.4 and 4.5.

FIGURE 4.2

PAX-E1

NUMBER OF COMPONENTS WITHIN CORE BY RADIAL REGION

Region Ident.	1	2	3	4	5	6	7	8	9	
Radius, Cm	15.747	20.445	25.391	32.491	34.294	36.689	39.480	41.719	43.804	Total
Fuel Element										
Code 18 (A3-C Fuel) WNCO	54									54
Code 39 WNCO									72	72
Code 49 WNCO								18	12	30
Code 59 WNCO								24		24
Code 69 WNCO							12	36		48
Code 79 WNCO							48			48
Code 89 WNCO							24			24
Code 99 WNCO	144	138	198	330	108	114	30			1062
Code 04[1] WNCO	18	6				36	60	48	54	222
Total	216	144	198	330	108	150	174	126	138	1584
Unfueled Element										
00	1									1
01	23	18	24	60	12	36	9	38	2	222
02	13	6	6				3	28	10	66
03									42	42
Total	37	24	30	60	12	36	12	66	54	331

(1) The code 04 element is a nineteen-hole unfueled graphite element. Since the code 04 elements occupy fueled element locations in the core, they are considered to be fueled elements.

FIGURE 4.3
NRX-A6

NUMBER OF COMPONENTS WITHIN CORE BY RADIAL REGIONS

		Radial Region (Outer Radius Given in cm)									
		15.747	20.445	25.391	32.491	34.294	36.689	39.480	41.719	43.804	Total
Region Identification		1	2	3	4	5	6	7	8	9	
Fuel	Element										
Code 11											
	WNCO									102	102
Code 12											
	WNCO									30	30
Code 13											
	WNCO								66	6	72
Code 14											
	Y-12								33		33
	WNCO								27		27
Code 15											
	Y-12							52			52
	WNCO							32			32
Code 16											
	Y-12						18	42			60
	WNCO						0	36			36
Code 17											
	Y-12						43	7			50
	WNCO						23	5			28
Code 18											
	Y-12	140					55				195
	WNCO	70					11				81
Code 19											
	Y-12	3	52	4		23					82
	WNCO	3	80	2		25					110
Code 20											
	Y-12		7	97	4	29					147
	WNCO		5	77	2	15					99
Code 21											
	Y-12			9	171	3					183
	WNCO			9	153	3					165
Total		216	144	198	330	108	150	174	126	138	1,584
Unfueled	Elements										
00 (1-Hole; TaC-Loaded)		6	0	0	18	6	8	0	0	0	38
01 (1-Hole)		19	19	26	27	6	19	9	51	9	185
02 (Multihole)		12	5	4	15	0	9	3	15	3	66
03 (Unfueled Partial)										42	42
Total		37	24	30	60	12	36	12	66	54	331

FIGURE 4.4

PAX-Q QUADRANT

NUMBER OF COMPONENTS WITHIN CORE BY RADIAL REGION

Region Ident.	1	2	3	4	5	6	7	8	9	
Radius, Cm	15.747	20.445	25.391	32.491	34.294	36.689	39.480	41.719	43.804	Total
Fuel Element										
Code 39 WNCO									18	18
Code 49 WNCO								4	3	7
Code 59 WNCO								7		7
Code 69 WNCO							2	7		9
Code 79 WNCO							13			13
Code 89 WNCO							7			7
Code 99 WNCO	37	35	50	80	28	28	8			266
Code 04 WNCO	4	2				8	16	12	14	56
Total	41	37	50	80	28	36	46	30	35	383

FIGURE 4.5

A6-Q QUADRANT

NUMBER OF COMPONENTS WITHIN CORE BY RADIAL REGION

Region Ident.	1	2	3	4	5	6	7	8	9	
Radius, Cm	15.747	20.445	25.391	32.491	34.294	36.689	39.480	41.719	43.804	Total
Fuel Element										
Code 11 WNCO									26	26
Code 12 WNCO									7	7
Code 13 WNCO								18	2	20
Code 14 WNCO								12		12
Code 15 Y-12							24			24
Code 16 WNCO						3	18			21
Code 17 Y-12						18	4			22
Code 18 WNCO	11					11				22
Code 18 Y-12	28					4				32
Code 19 WNCO		6			13					19
Code 19 Y-12	2	27	1							30
Code 20 WNCO		1	7		13					21
Code 20 Y-12		3	36	1						40
Code 21 WNCO				20						20
Code 21 Y-12			6	59	2					67
Total	41	37	50	80	28	36	46	30	35	383

Figures 4.6 and 4.7 are the material mass inventories for the PAX-E1 and NRX-A6 reactor, respectively. The masses of materials in the PAX-Q quadrant are given in Figure 4.8, and the masses of materials in the A6-Q quadrant are given in Figure 4.9.

4.2.2 Regions Outside the Core

The masses of materials outside the core of PAX-E1 are given in Figure 4.10. The masses of components outside the core of NRX-A6 are given in Figure 4.11. The mass differences between PAX-E1 and NRX-A6 existed because of the fact that PAX-E1 was constructed as a mockup of NRX-A6. The filler strip region in PAX-E1 consisted of filler strips and a bundling mechanism, whereas the same region in NRX-A6 contained filler strips, filler tiles, a friction plane and an impedance wrapper. In the lateral support region, PAX-E1 had graphite liner plates, whereas NRX-A6 contained inner and outer seal segments, and insulation segments. The only lateral support hardware in the reflector region of PAX-E1 was the Inconel-718 lateral support springs. Also, the NRX-A6 had a complete lateral support system which includes lateral support springs, along with associated hardware, such as plungers, plunger springs, seal rings, retaining latches, etc.

With the exception of the lateral support hardware, the PAX-E1 and NRX-A6 were assumed to have no mass differences in the control drum or reflector regions. This assumption was made with full knowledge that one reflector ring and one control drum were changed from the PAX-E1 configuration to the NRX-A6 configuration. Measured masses for the two reflectors indicate that these differences were negligible. The PAX-E1 and NRX-A6 cluster plates

FIGURE 4.6

PAX-E1

MATERIAL MASSES BY REGION, KG

(AT ROOM TEMPERATURE)

Region Identification Radius, cm	1 15.747	2 20.445	3 25.391	4 32.491	5 34.294	6 36.689	7 39.480	8 41.719	9 43.804	Total
Material										
Carbon										
Fueled Elements	115.238	76.293	104.582	174.303	57.045	80.630	94.755	69.230	76.192	848.268
Unfueled Elements	22.075	14.459	18.157	36.987	7.397	22.192	7.229	39.117	6.827	174.450
Pyrographite Sleeves	3.550	2.303	2.879	5.757	1.151	3.454	1.151	6.333	1.151	27.729
Positive Shims(6)	----	----	----	----	----	----	----	----	----	
Partial Elements	0.0	0.0	0.0	0.0	0.0	0.0	0.0	0.0	20.274	20.274
Total Carbon	140.863	93.055	125.618	217.047	65.593	106.276	103.135	114.680	104.454	1070.721
Uranium(1)	23.340	16.864	24.196	40.327	13.198	13.931	11.447	5.145	3.557	152.005
Niobium(2), Coating										
Bore										
Fueled Elements	9.179	6.258	8.979	14.966	4.898	5.170	4.599	3.426	3.690	61.165
Unfueled Elements	0.612	0.0	0.0	0.0	0.0	0.0	0.0	0.0	0.0	0.612
Matrix	0.0	0.0	0.0	0.0	0.0	0.0	0.0	0.0	0.0	0.0
External										
Fueled Elements	0.00004	0.0	0.0	0.0	0.0	0.0	0.0	0.0	0.0	0.00004
Unfueled Elements	0.0005	0.0	0.0	0.0	0.0	0.0	0.0	0.0	0.0	0.0005
Partial Elements	0.0	0.0	0.0	0.0	0.0	0.0	0.0	0.0	0.296	0.296
Total Niobium	9.792	6.258	8.979	14.966	4.898	5.170	4.599	3.426	3.986	62.074
Molybdenum(2), Coating	0.0	0.0	0.0	0.0	0.0	0.0	0.0	0.0	0.0	0.0
Tantalum	0.075	0.0	0.0	0.0	0.0	0.0	0.0	0.0	0.0	0.075
Stainless Steel(3)	1.053	0.683	0.854	1.707	0.341	1.024	0.341	1.877	1.304	9.184
Inconel-X750(4)	2.891	1.875	2.344	4.688	0.938	2.813	0.938	5.157	0.938	22.582
Hydrogen(5)	0.0014	0.0009	0.0013	0.0022	0.0007	0.0011	0.0010	0.0011	0.0010	0.0107
Niobium Wires	2.336	1.602	2.136	3.871	1.135	1.602	2.002	1.713	1.680	18.077
Molybdenum Wires	1.970	1.351	1.802	3.266	0.956	1.351	1.690	1.445	1.417	15.248

(1) Uranium masses based on a 52 inch length.
(2) Material is reactivity weighted.
(3) Tube liner weights only; does not include orifice jets.
(4) Weight for entire length of the tie rod.
(5) Hydrogen weight assumed to be 10 ppm of the total carbon weight.
(6) Positive shim weights are included in unfueled element weights.

FIGURE 4.7

NRX-A6

MATERIAL MASSES BY RADIAL REGION, KG

(At Room Temperature)

Region Identification	1	2	3	4	5	6	7	8	9	
Radius, cm	15.747	20.445	25.391	32.491	34.294	36.689	39.480	41.719	43.804	Total
Material										
Carbon										
Fueled Elements	115.097	76.36	104.356	174.215	57.264	80.446	94.324	68.482	75.246	846.291
Unfueled Elements	22.419	14.587	18.259	36.373	7.298	21.834	7.288	40.102	7.288	175.448
Pyrographite Sleeves	3.510	2.277	2.846	5.691	1.138	3.415	1.138	6.260	1.138	27.413
Positive Shims	0.185	0.07	0.062	0.231	0.0	0.139	0.046	0.231	0.046	1.017
Partial Elements	0.0	0.0	0.0	0.0	0.0	0.0	0.0	0.0	20.477	20.477
Total Carbon	141.211	93.302	126.023	216.510	65.700	105.834	102.796	115.075	104.195	1070.646
Uranium[1]	23.908	17.28	25.414	44.637	13.438	14.831	11.908	5.308	3.660	160.388
Niobium[2] Coating										
Bore										
Fueled Elements	10.603	7.05	9.986	16.647	5.427	7.354	8.352	6.279	6.867	78.569
Unfueled Elements	0.256	0.16	0.211	0.415	0.083	0.250	0.084	0.463	0.084	2.014
Matrix	0.194	0.31	0.366	0.939	0.009	0.122	0.0	0.179	0.0	2.125
External										
Fueled Elements	0.003	0.002	0.003	0.005	0.002	0.002	0.002	0.522	1.031	1.572
Unfueled Elements	0.758	0.493	0.619	1.241	0.254	0.743	0.246	1.354	0.246	5.954
Partial Elements	0.0	0.0	0.0	0.0	0.0	0.0	0.0	0.0	0.150	0.150
Total Niobium	11.814	8.033	11.185	19.247	5.775	8.471	8.684	8.797	8.378	90.384
Molybdenum[2], Coating	0.949	0.635	0.819	1.449	0.446	0.645	0.721	0.513	0.528	6.705
Tantalum	0.446	0.0	0.0	1.339	0.446	0.595	0.0	0.0	0.0	2.826
Stainless Steel[3]	1.030	0.668	0.835	1.670	0.334	1.002	0.334	1.837	0.334	8.044
Inconel-718[4]	3.027	1.964	2.455	4.909	0.982	2.946	0.982	5.400	0.982	23.647
Hydrogen[5]	0.0014	0.0009	0.0013	0.0022	0.0007	0.0011	0.0010	0.0012	0.0010	0.0108

(1) Uranium masses based on a 52 inch length.
(2) Material is reactivity-weighted.
(3) Tube liner masses only; does not include orifice jets.
(4) Mass for entire length of tie rod.
(5) Hydrogen weight assumed to be 10 ppm of the total carbon weight.

FIGURE 4.8

PAX-Q QUADRANT

MATERIAL MASSES(1) BY REGION, KG

(AT ROOM TEMPERATURE)

Region Identification Radius, cm	1 15.747	2 20.445	3 25.391	4 32.491	5 34.294	6 36.689	7 39.480	8 41.719	9 43.804	Total
Material										
Carbon										
Fueled Element	21.780	19.595	26.379	42.207	14.772	19.290	24.995	16.457	19.308	204.783
Uranium(2)	4.522	4.277	6.110	9.776	3.422	3.422	3.033	1.176	0.888	36.626
Niobium(3), Coating										
Bore										
Fueled Elements	1.677	1.587	2.267	3.626	1.269	1.269	1.206	0.810	0.956	14.667
Matrix	0.0	0.0	0.0	0.0	0.0	0.0	0.0	0.0	0.0	0.0
External										
Fueled Elements	0.0	0.0	0.0	0.0	0.0	0.0	0.0	0.0	0.0	0.0
Total Niobium	1.677	1.587	2.267	3.626	1.269	1.269	1.206	0.810	0.956	14.667
Molybdenum, Coating	0.0	0.0	0.0	0.0	0.0	0.0	0.0	0.0	0.0	0.0
Niobium Wires	0.592	0.406	0.541	0.981	0.288	0.406	0.508	0.434	0.426	4.582
Molybdenum Wires	0.481	0.330	0.440	0.797	0.233	0.330	0.412	0.352	0.345	3.720

(1) Material masses are given for fueled elements only. The unfueled elements and core hardware (tie rods, tube liners, etc.,) in the test quadrant are the same as in the 360° PAX inventory. No unfueled elements or hardware was changed in the test quadrant.
(2) Uranium masses are based on a 52.0 inch length.
(3) Material is reactivity weighted.

FIGURE 4.9

A6-Q QUADRANT

MATERIAL MASSES(1) BY REGION, KG

(AT ROOM TEMPERATURE)

Region Identification Radius, cm	1 15.747	2 20.445	3 25.391	4 32.491	5 34.294	6 36.689	7 39.480	8 41.719	9 43.804	Total
Material										
Carbon Fueled Elements	21.802	19.637	26.492	42.205	14.841	19.250	24.834	16.283	19.004	204.348
Uranium(2)	4.661	4.357	6.394	11.156	3.504	3.581	3.101	1.239	0.924	38.917
Niobium(3), Coating Bore Fueled Elements	1.971	1.807	2.323	3.782	1.287	1.687	2.222	1.694	2.208	18.981
Matrix External	0.0	0.0	0.0	0.0	0.0	0.0	0.0	0.0	0.0	0.0
Fueled Elements	0.0006	0.0006	0.0008	0.0012	0.0004	0.0005	0.0007	0.1864	0.3617	0.5529
Total Niobium	1.9716	1.8076	2.3238	3.7832	1.2874	1.6875	2.2227	1.8804	2.5697	19.5339
Molybdenum(3), Coating	0.183	0.156	0.216	0.380	0.141	0.162	0.207	0.132	0.135	1.712

(1) Material masses are given for fueled elements only. The unfueled elements and core hardware (tie rods, tube liners, etc.) in the test quadrant are the same as in the 360° PAX inventory. No unfueled elements or hardware was changed in the test quadrant.

(2) Uranium masses based on a 52.0 inch length.

(3) Material is reactivity weighted.

FIGURE 4.10

PAX-E1

REFLECTOR REGION MASSES[1]

Region	Material	Mass, Kg
Filler Strip	Graphite	87.32
	Stainless Steel	10.59
Lateral Support	Graphite	110.95
	Aluminum	1.98
Beryllium Reflector		
Hardware	Inconel-718	36.14
	Plastic Tape	0.33
	Teflon Tape	0.16
Reflector	Beryllium	884.50
	Titanium	14.67
Control Drums	Beryllium	199.85
	Aluminum	18.11
	Boron-10	1.03
Cluster Plate	Gd Stainless Steel	8.50
	Stainless Steel	20.30
	Aluminum	2.00
	Inconel	0.04
Support Block	Graphite	37.61
	Stainless Steel	4.00
	Molybdenum	1.46
Support Plate	Aluminum	122.47
Pressure Vessel	Aluminum	255.33

(1) Mass for 52.0 inch active core length.

FIGURE 4.11

NRX-A6

REFLECTOR REGION MASSES(1)

Region	Material	Mass, Kg
Filler Strip	Graphite	95.48
	Niobium	0.76
	Paraffin	0.012
	Silicone Grease	0.069
Lateral Support	Graphite	115.08
	Niobium	0.001
Beryllium Reflector Hardware	Graphite	5.30
	Inconel-718	37.11
	Stainless Steel	0.69
	Nispan	1.99
	Titanium	2.94
	Copper	1.54
	Aluminum	11.93
Reflector	Beryllium	884.50
	Titanium	14.67
Control Drums	Beryllium	199.85
	Aluminum	18.11
	Boron-10	1.03
Cluster Plate	Ag-In-Cd	11.47
	Stainless Steel	20.32
	Aluminum	2.49
	Inconel	0.52
Support Block	Graphite	27.53
	Niobium	7.69
	Stainless Steel	0.21
	Molybdenum	1.47
	Tungsten	4.29
	ThO_2	0.07
	Inconel	1.27
Support Plate	Aluminum	212.29
Pressure Vessel	Aluminum	239.24
	Copper	16.09

(1) Mass for 52.0 inch active core length.

were assumed, respectively, to have the same mass as the plates in the NRX-A4 and NRX-A5 reactors. The miscellaneous cluster plate hardware in PAX-E1 was assumed to have the same material masses as the hardware which existed in the A2-PAX reactor (See Reference 3). The masses of NRX-A6 cluster plate hardware were assumed to be the same as those which existed in the NRX-A2 reactor (See Reference 3).

4.3 Uncertainties in Reactor Masses

Figure 4.12 shows the reactivity uncertainty which occurs because of uncertainties in reactor masses. The statistical sum of these uncertainties was found to be $\pm 0.38\$$.

The uncertainty in a mass was based on the following three factors:

1. Accuracy of the measuring instruments used,
2. Human error involved in measurement and calculations, and
3. Accuracy of the sampling techniques, i.e., error caused by the measured mass of a group of components not being representative of all the components of that type.

The mass uncertainties associated with fuel inventories involve four sets of inventories, the PAX-E1, PAX-QE, A6-QE, and NRX-A6 fuel. This occurs because of the manner in which the fuel reactivity differences are determined (See Sections 3.0 and 6.1 for details). Therefore, the fuel mass uncertainties reported in Figure 4.12 reflect the net possible error in all four sets of inventories.

FIGURE 4.12

REACTIVITY UNCERTAINTY DUE TO MASS UNCERTAINTIES

NRX-A6 MINUS PAX-E1

Region	Material	Mass Difference & Uncertainty, kg	Reactivity Coefficient, ¢/kg	Reactivity Uncertainty, ¢
Core	Fueled Elements			
	Carbon	1.977 ± 4.0	5.04	±20.2
	Uranium	8.381 ± 1.0	15.01	±15.0
	Niobium	3.024 ± 3.0	-5.55	±16.7
	Molybdenum(1)	± 0.6	-13.68	± 8.2
	Unfueled Elements			
	Carbon	1.201 ± 3.0	5.04	±15.1
	Tantalum	2.751 ± 0.05	-61.72	± 3.0
	Niobium	7.671 ± 1.0	-5.55	± 5.6
	Hydrogen	± 0.001	670.0	± 0.1
	Hardware			
	Positive Shims	1.017 ± 0.0	5.04	± 0.0
	Pyrographite Sleeves	-0.317 ± 0.0	5.04	± 0.0
	Tie Rods	1.065 ± 0.1	——	± 0.1
	Tube Liners	-0.178 ± 0.0	-0.24	± 0.0
Filler Strip	Carbon	8.161 ± 4.0	+3.0	±12.0
	Niobium	0.757 ± 0.1	-4.2	± 0.4
	Stainless Steel	-10.592 ± 1.0	-3.28	± 3.3
	Paraffin	0.0122	70.0	± 0.8
	Silicone Grease	0.0686		
Lateral Support	Carbon	4.129 ± 1.0	+2.9	± 2.9
	Niobium	0.001 ± 0.0		± 0.0
	Aluminum	-1.975 ± 0.2	+0.26	± 0.0
Beryllium Reflector	Inconel-718	0.968 ± 0.1	-0.25	± 0.0
	Carbon	5.301 ± 0.5	+3.5	± 1.8
	Titanium	2.944 ± 0.3	-2.0	± 0.6
	Stainless Steel	0.691 ± 0.1	-0.25	± 0.0
	Nispan	1.986 ± 0.2	-0.25	± 0.0
	Copper	1.539 ± 0.1	-0.25	± 0.0
	Aluminum	11.929 ± 0.5	+0.37	± 0.2
	Plastic Tape	-0.326	10.0	± 0.7
	Teflon Tape	-0.156		
Reflector	Beryllium	0.0 ± 0.5	+2.2	± 1.1
	Titanium	0.0 ± 0.0	-2.0	± 0.0
Control Drums	Beryllium	0.0 ± 0.0	+2.2	± 0.0
	Aluminum	0.0 ± 0.0	+0.37	± 0.0
	Boron-10	0.0 ± 0.0		± 0.0
Cluster Plate	Ag-In-Cd	11.465	——	± 0.0
	Cd	-8.499	——	
	Stainless Steel	-0.02 ± 1.5	0.67	± 1.0
	Aluminum	0.495 ± 0.0	——	± 0.0
	Inconel	0.47 ± 0.0	0.81	± 0.0
Support Block	Carbon	-10.088 ± 1.0	1.36	± 1.4
	Niobium	7.692 ± 1.0	0.41	± 0.4
	Stainless Steel	-3.785 ± 0.0	0.45	± 0.0
	Molybdenum	0.011 ± 0.0	0.49	± 0.0
	Tungsten	4.288 ± 0.5	0.18	± 0.0
	ThO_2	0.068 ± 0.0		± 0.0
	Inconel	1.27 ± 0.0	0.65	± 0.0
Support Plate	Aluminum	89.813 ± 5.0	0.20	± 1.0
			Statistical Sum of Uncertainties	±37.7¢

(1) The PAX-E1 mass includes 31 and 40 mil molybdenum wires which differ in self-shielding factor from the molybdenum in NRX-A6

SECTION 5.0

(CRD) REACTIVITIES AND REACTIVITY COEFFICIENTS

The reactivity effects and the reactivity coefficients used in the NRX-A6/PAX-E1 reactivity comparison were obtained from experimental measurements made in the PAX-E reactor configuration which simulated the NRX-A6 reactor. Measurements were also made in previous PAX configurations which simulated the NRX-A2 through NRX-A5 reactors. In addition, some of the reactivity effects were determined from basic neutronic calculations.

The PAX-E test series consisted of three separate reactor configurations which simulated NRX-A6 conditions. The following is a description of each of these configurations.

Figure 5.1 shows the first reactor configuration which simulated the NRX-A6. This configuration is identified as the PAX-EO reactor configuration. The core of this reactor configuration consisted of NRX-A2 production fuel into which a quadrant of NRX-A6 build 1 fuel was substituted. The NRX-A6 build 1 fuel is the fuel that was initially manufactured for the NRX-A6 reactor. This fuel had a uranium zone loading similar to the NRX-A5 and did not employ an increased number of fuel loadings to flatten the radial power shape. The NRX-A6 filler strip and lateral support region was simulated in the PAX-EO with mockup filler strips and graphite liner plates. The reflector region of the NRX-A6 was simulated in the following manner:

1. One quadrant (90°) of the PAX-EO reflector consisted of three beryllium sectors from the NRX-A2 reactor. These sectors had been modified to closely represent the NRX-A6 beryllium reflector in the mass and distribution of beryllium.

Astronuclear Laboratory

FIGURE 5.1

PAX-EO REACTOR CONFIGURATION

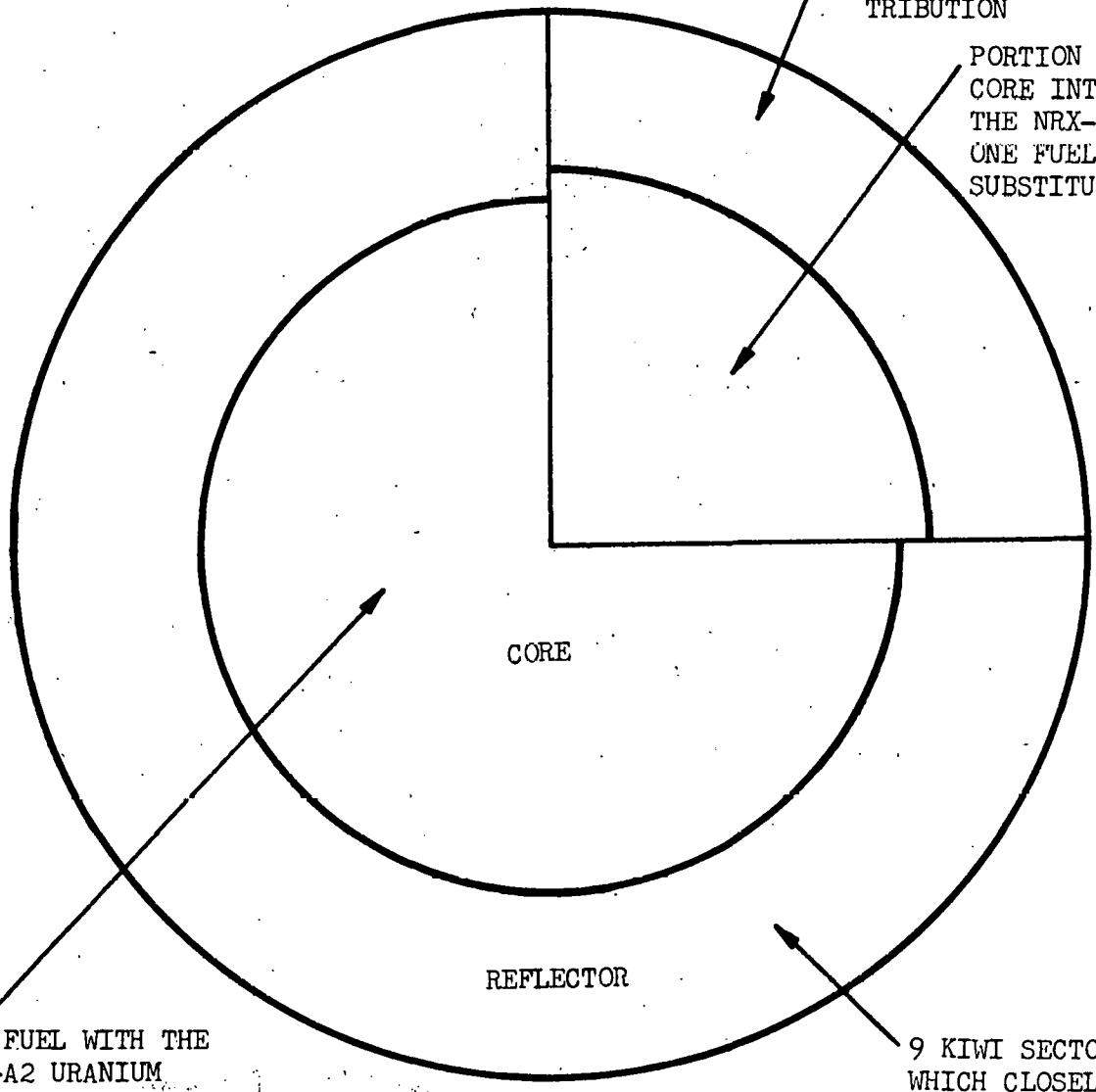

2. The remaining 270° of the PAX-EO reflector consisted of 9 beryllium sectors from a KIWI reactor. These sectors had also been modified to simulate the NRX-A6 reflector; however, the KIWI sector closely simulated the NRX-A6 reflector in the total mass of beryllium and not in its distribution.

Figure 5.2 shows the second reactor configuration in which NRX-A6 reactivity experiments were performed. This configuration is identified as the PAX-E1 reactor. The core of this reactor consisted of NRX-A2 production fuel which had been modified to represent the multi-zoned, power-flattening, uranium distribution of the NRX-A6 rebuild fuel. This was accomplished by replacing fueled elements with nineteen-hole unfueled graphite elements. (The nineteen-hole unfueled elements have been designated as loading code 04 fuel). Into this core was substituted a quadrant of preproduction NRX-A6 fuel which was similar to the final fuel loading distribution for the NRX-A6 rebuild fuel. Again as in the previous configuration, the NRX-A6 filler strips and lateral support region were simulated with mockup filler strips and graphite liner plates. However, unlike the previous configuration the PAX-E1 reactor contained the actual beryllium reflector rings and control drums which were used in the NRX-A6 reactor. The only components missing in the mockup of the NRX-A6 reflector were the lateral support hardware components, other than the springs.

Figure 5.3 shows the third reactor configuration in which experimental measurements for the NRX-A6 reactor were made. This configuration is

FIGURE 5.2

PAX-E1 REACTOR CONFIGURATION

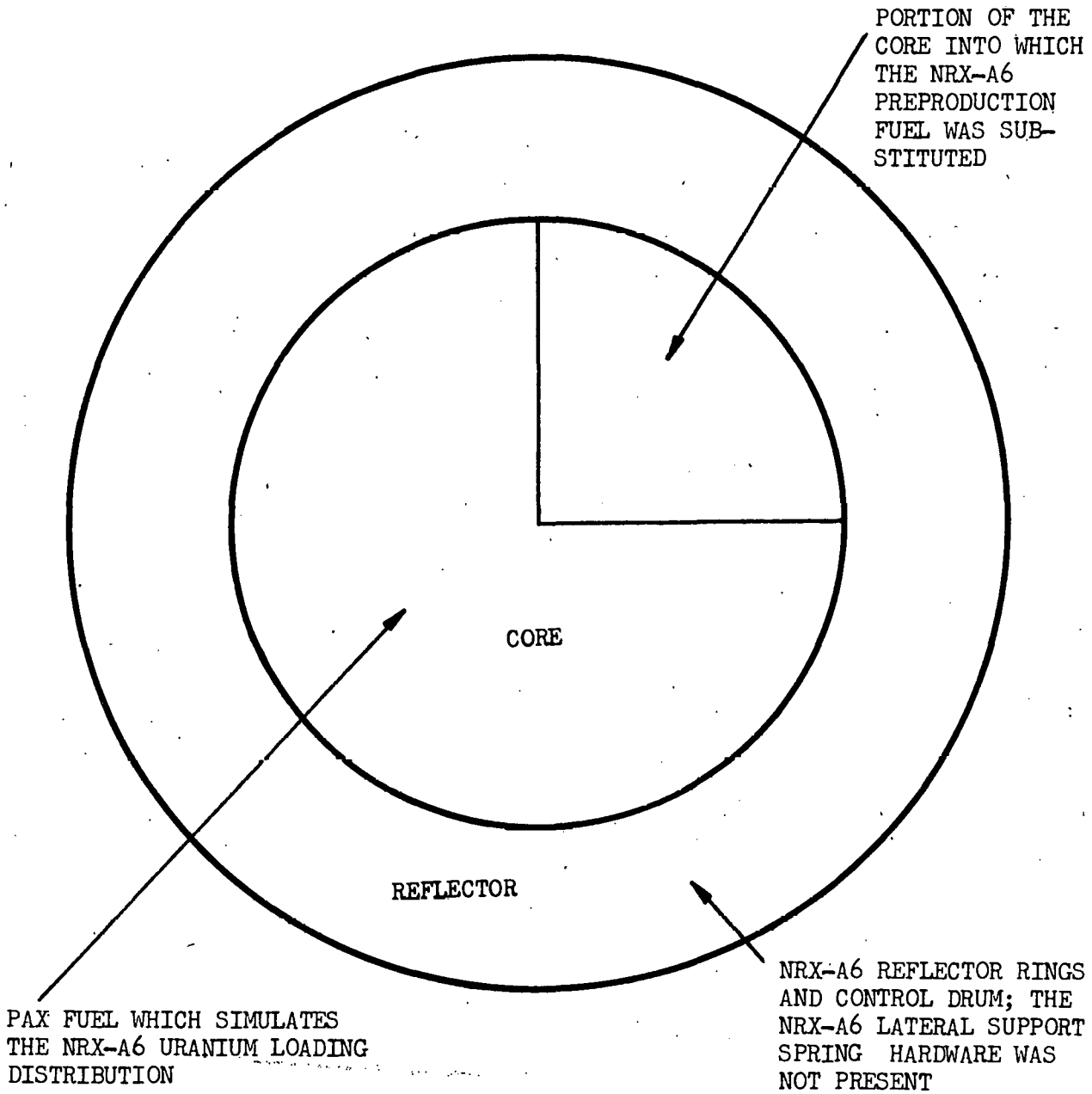

FIGURE 5.3
PAX-E2 REACTOR CONFIGURATION

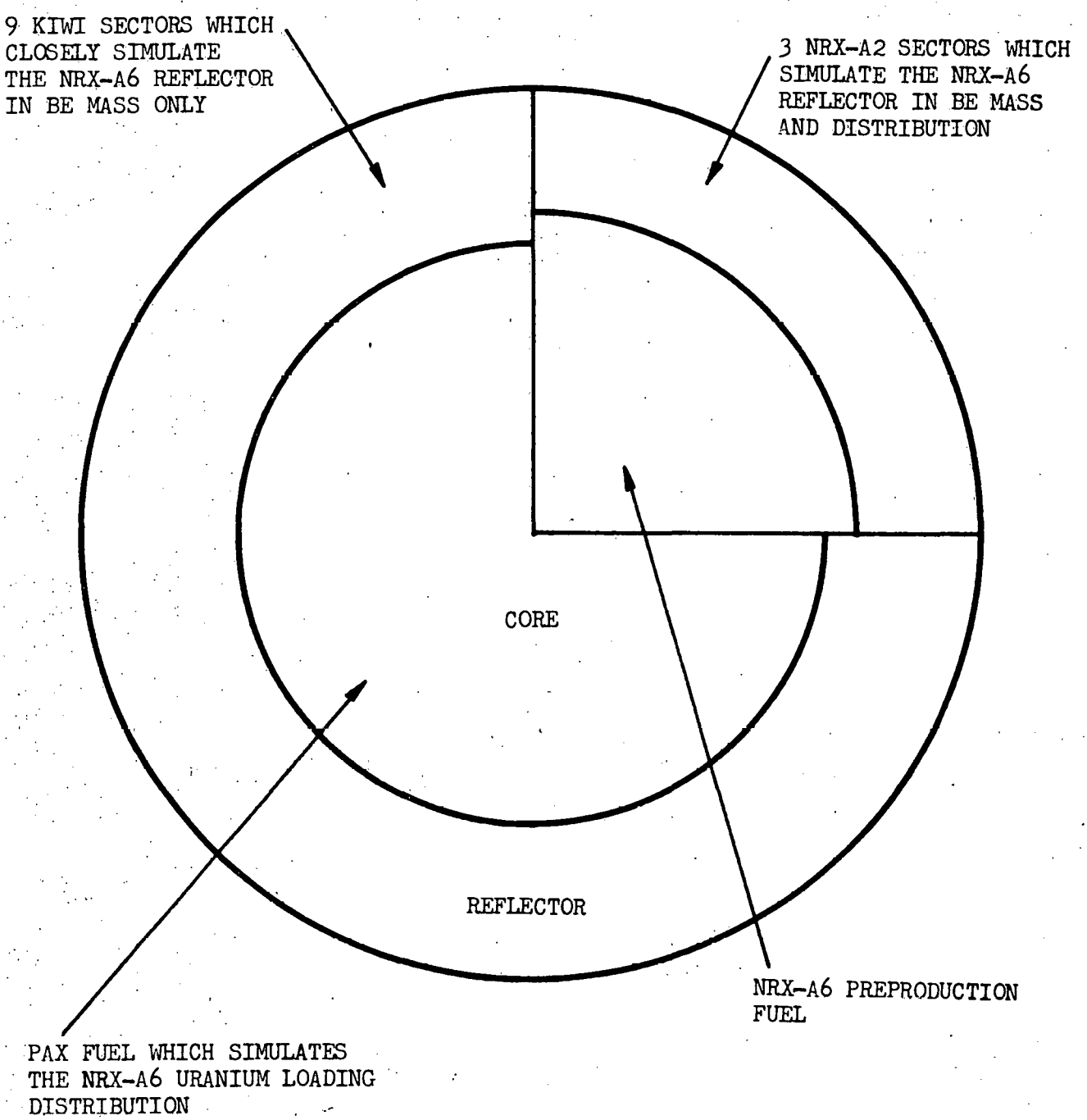

identified as the PAX-E2 reactor. This reactor configuration had points in common with both of the previous two configurations. The PAX-E2 reactor had the core configuration of the PAX-E1 reactor; that is, the reactor had one quadrant (90°) of NRX-A6 preproduction fuel and three quadrants (270°) of NRX-A2 production fuel which had been modified to simulate the NRX-A6 power-flattening uranium loading distribution. However, unlike the PAX-E1 reactor, the PAX-E2 reactor employed the reflector mockup that had been used in the PAX-E0 configuration.

In addition to the variations in the PAX-E reactor configuration described above, a thin set and thick set of beryllium liner plates existed for the PAX-E0 and PAX-E2 mockup of the NRX-A6 beryllium reflector. These variations in the PAX-E reactor configuration made it possible to have twelve different reactor configurations in which reactivity effects could be measured. The maximum number of configurations in which a given reactivity coefficient was measured is five.

5.1 Core Reactivity Coefficients

Figures 5.4 through 5.8 show, respectively, the reactivity coefficients of carbon, uranium, niobium, molybdenum, and tantalum as a function of radial position. Figures 5.9 and 5.10 show, respectively, the reactivity coefficients of molybdenum and niobium as a function of wire diameter. Figure 5.11 shows the volume-averaged reactivity coefficients of carbon, uranium, niobium, tantalum, molybdenum, stainless steel, Inconel 718, hydrogen, iron, nickel, and chromium.

The radial reactivity coefficient of carbon and uranium (Figure 5.4 and 5.5) was obtained in the quadrant of the PAX-E1 reactor configuration which

FIGURE 5.4

CARBON REACTIVITY COEFFICIENT AS A FUNCTION OF RADIAL POSITION

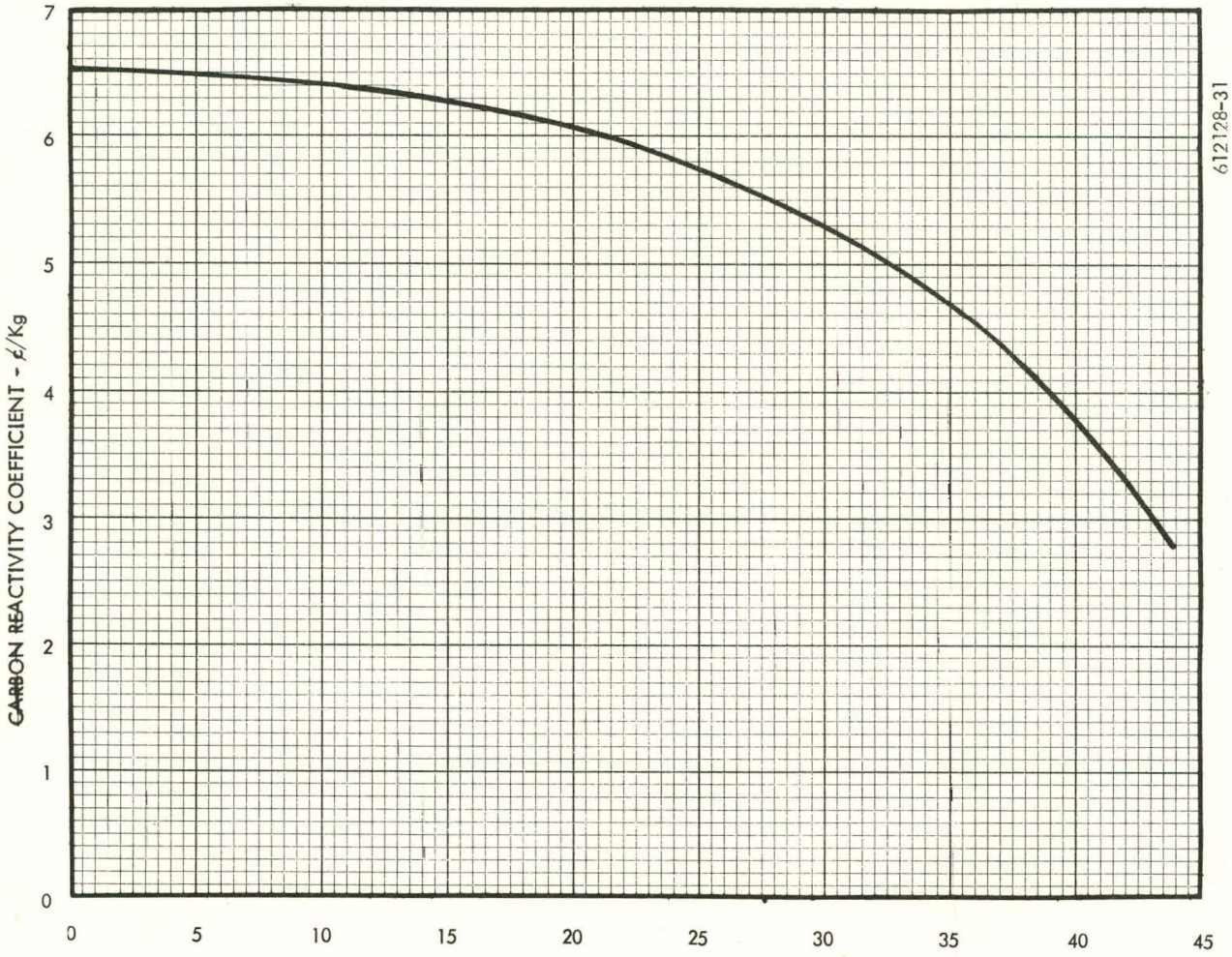

CONFIDENTIAL RESTRICTED DATA Atomic Energy Act of 1954

FIGURE 5.5

URANIUM REACTIVITY COEFFICIENT AS A FUNCTION OF RADIAL POSITION

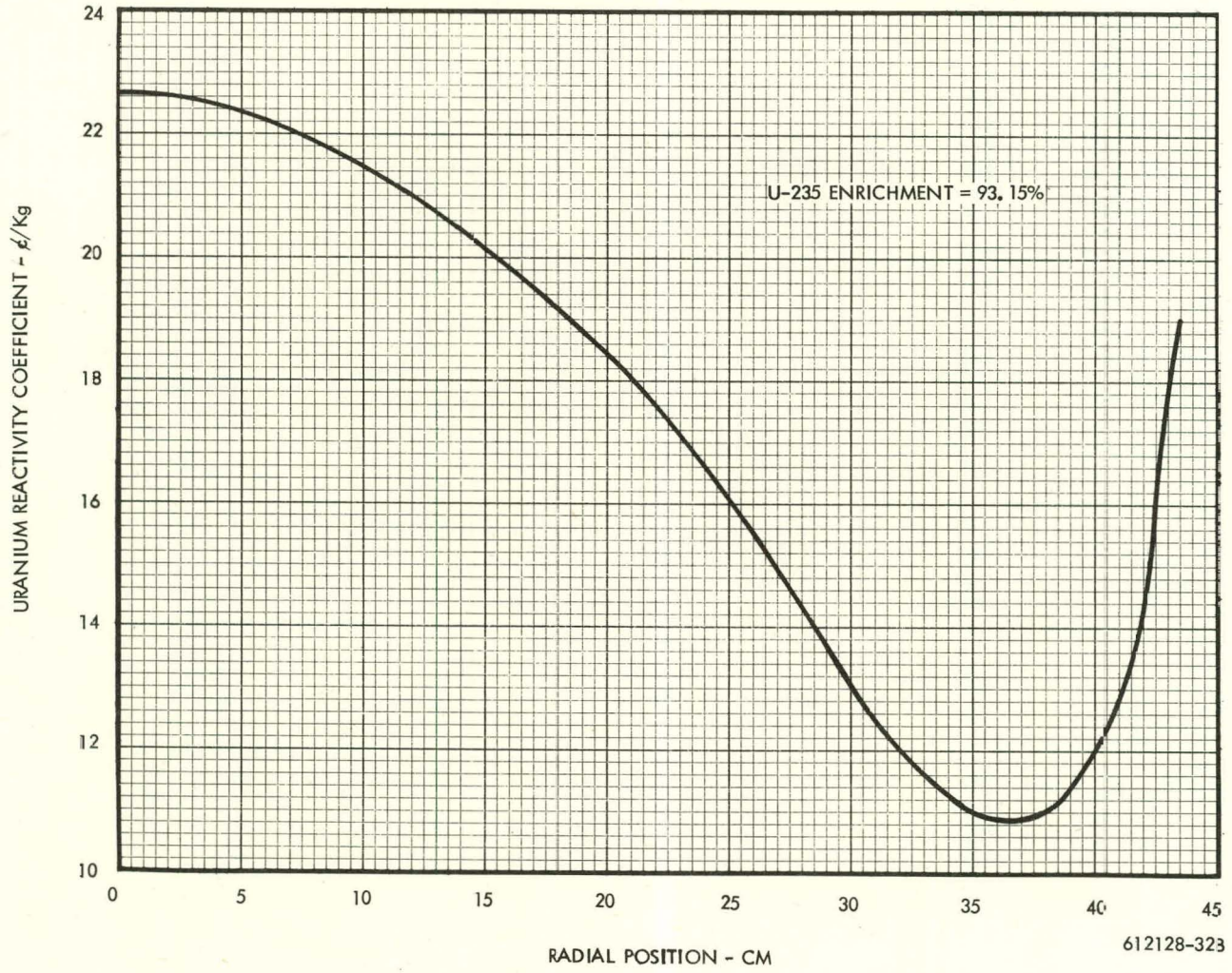

CONFIDENTIAL RESTRICTED DATA
This material contains information affecting the National Defense of the United States within the meaning of the Atomic Energy Act of 1954

FIGURE 5.6

NIOBIUM REACTIVITY COEFFICIENT AS A FUNCTION OF RADIAL POSITION

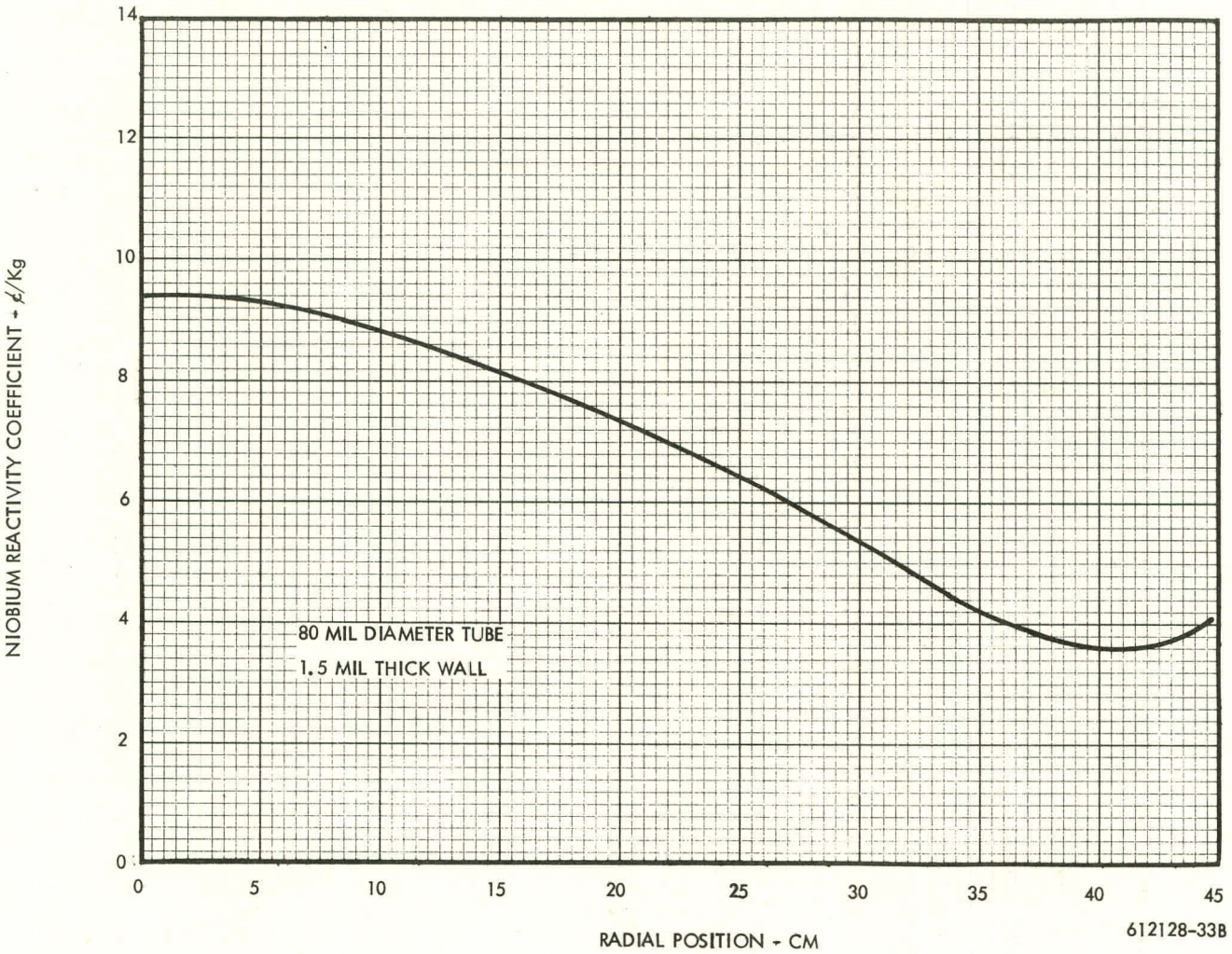

CONFIDENTIAL RESTRICTED DATA Atomic Energy Act of 1954

FIGURE 5.7

MOLYBDENUM FEACTIVITY COEFFICIENT AS A FUNCTION OF RADIAL POSITION

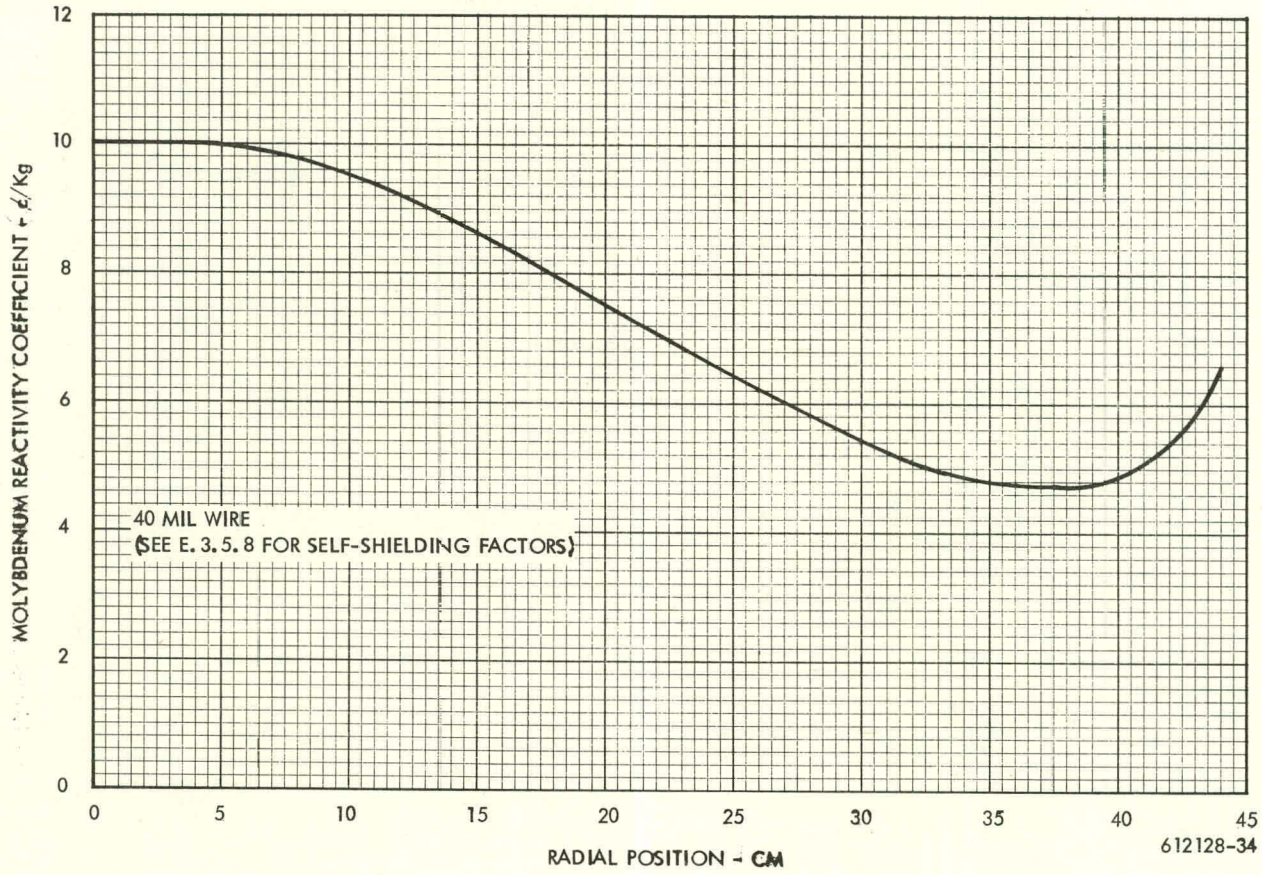

FIGURE 5.8

TANTALUM REACTIVITY COEFFICIENT AS A FUNCTION OF RADIAL POSITION

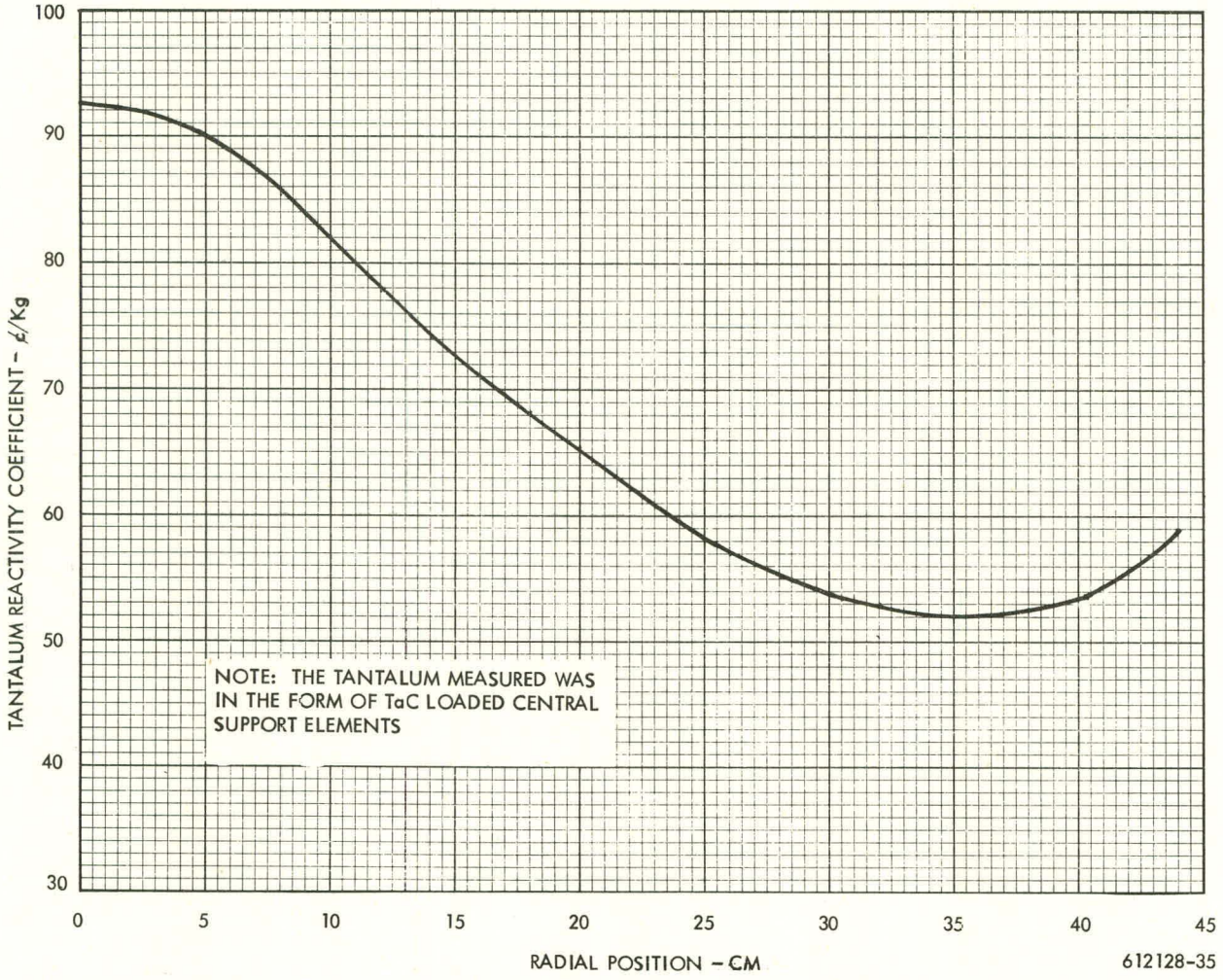

FIGURE 5.9

MOLYBDENUM REACTIVITY COEFFICIENT AS A FUNCTION OF WIRE DIAMETER

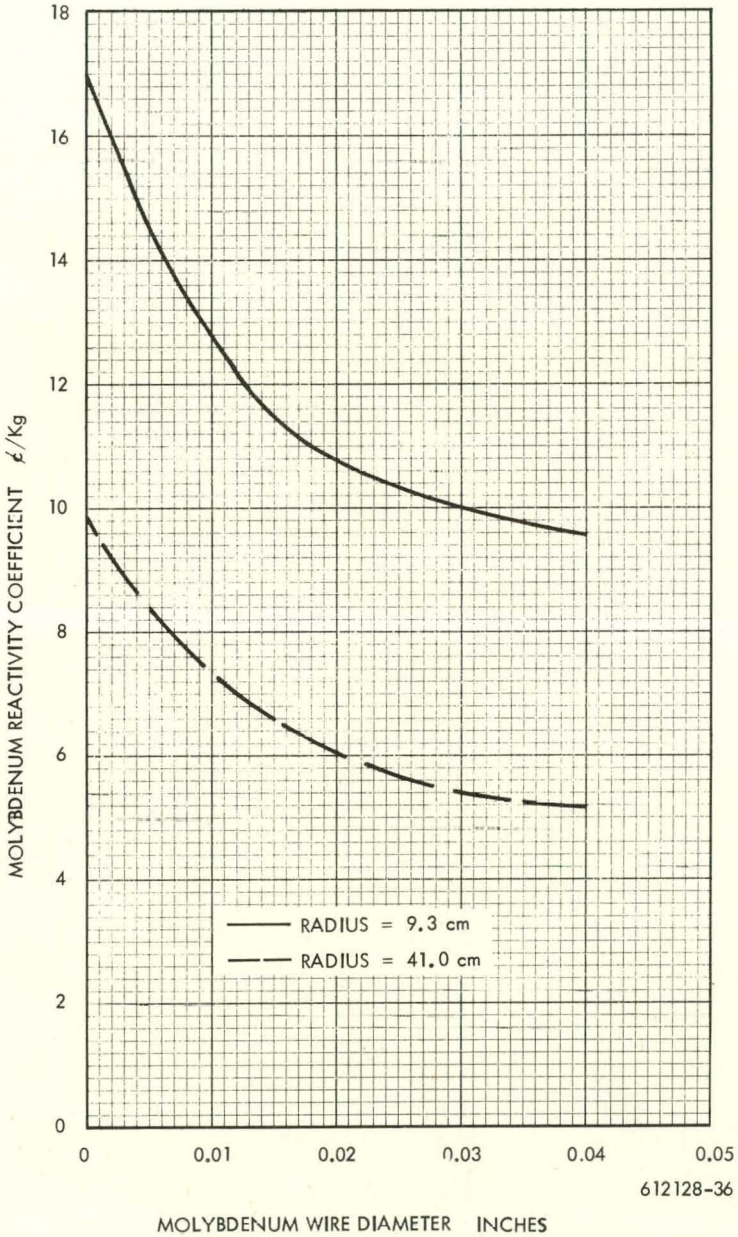

FIGURE 5.10

NIOBIUM REACTIVITY COEFFICIENT AS A FUNCTION OF NIOBIUM THICKNESS

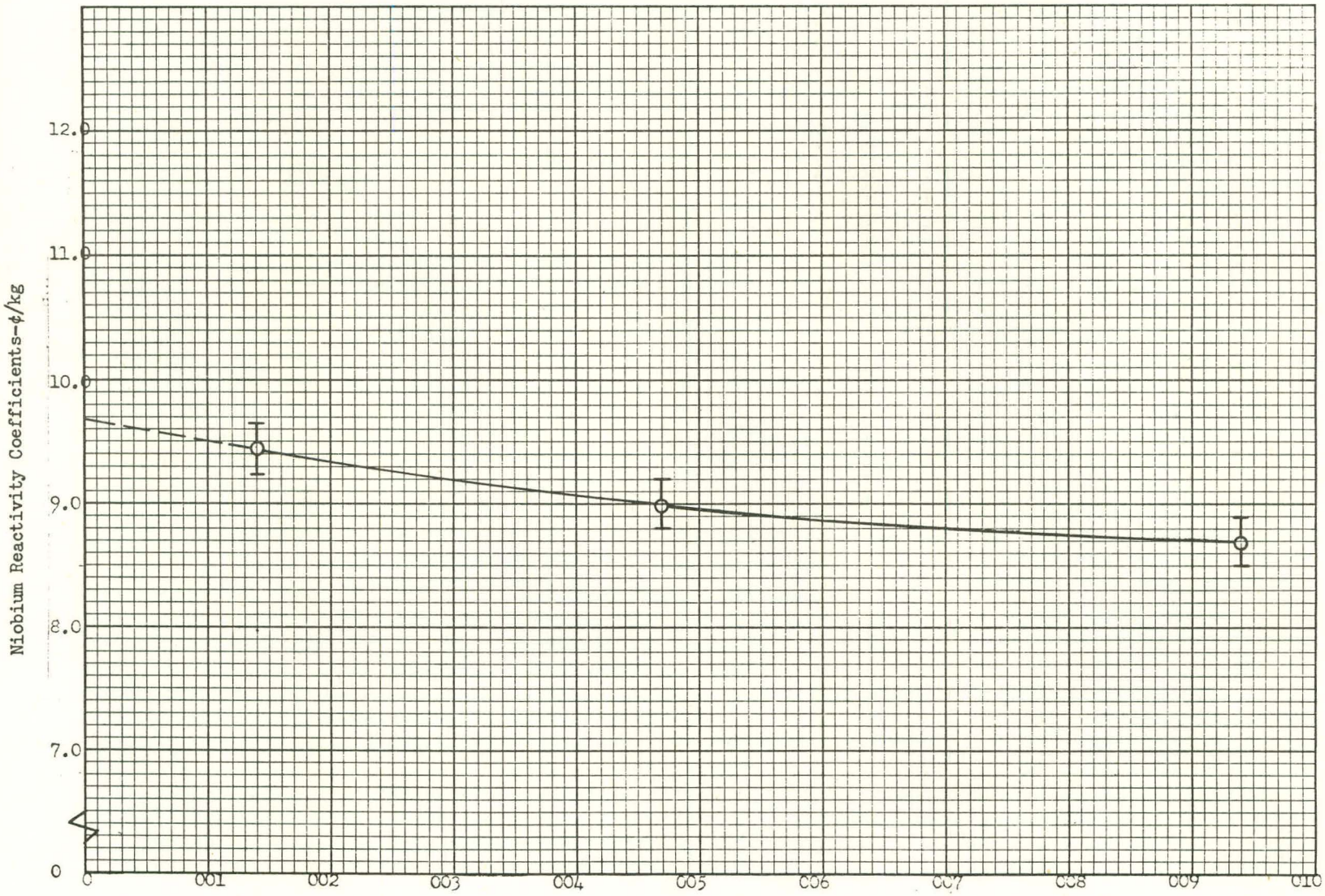

FIGURE 5.11

NRX-A6

AVERAGE REACTIVITY COEFFICIENTS FOR CORE REGIONS

	Region Average Reactivity Coefficient (ϕ/Kg)[1]									
Region Radius, cm	15.747	20.445	25.391	32.491	34.294	36.689	39.480	41.719	43.804	Core Average
Region Identification	1	2	3	4	5	6	7	8	9	
Carbon	6.38	6.13	5.88	5.39	4.93	4.63	4.18	3.66	3.14	5.04
Uranium	21.26	19.10	16.98	13.61	11.36	10.86	11.07	12.55	16.73	15.01
Niobium	-8.70	-7.62	-6.77	-5.49	-4.59	-4.19	-3.80	-3.66	-3.77	-5.55
Tantalum	-80.56	-67.40	-60.65	-54.86	-52.37	-52.02	-52.60	-54.02	-56.72	-61.72
Molybdenum	-16.83	-15.41	-14.32	-13.12	-12.51	12.33	-12.22	-12.46	-13.19	-13.68
Stainless	----	----	----	----	----	----	----	----	----	-0.24
Inconel-718	----	----	----	----	----	----	----	----	----	-1.21
Hydrogen	----	----	----	----	----	----	----	----	----	670.00
Iron	----	----	----	----	----	----	----	----	----	-0.18
Nickel	----	----	----	----	----	----	----	----	----	-0.96
Chromium	----	----	----	----	----	----	----	----	----	-0.13

(1) The coefficients for carbon, uranium, niobium, tantalum, nickel, molybdenum, and hydrogen are measured. The remainder are wholly or in part calculated. Other measured reactivity coefficients are given in WANL-TME-878, "NRX-A2 Reactivity and Shimming", July, 1964.

contained NRX-A6 fuel. The radial reactivity coefficient (Figure 5.6) of niobium was obtained in the quadrant of the PAX-E2 reactor configuration which contained NRX-A6 fuel. The radial reactivity coefficient (Figure 5.7) of molybdenum was obtained in the NRX-A6 build 1 fuel portion of the PAX-EO core. The radial reactivity coefficient of tantalum was based primarily on the worth of tantalum obtained in reshimming the PAX-El reactor configuration from the initial cold critical control drum position to the desired control drum position of 88°.

Since the best set of NRX-A6 core reactivity coefficients were measured in several reactor configurations and all of these configurations may have been affected by interaction effects between the various types of fuel and reflectors involved, it was necessary to perform numerous one-dimensional transport calculations to assure the compatibility of the coefficients used. It was found from these calculations that there was no essential difference between the coefficients used and those that would have been measured if all of the experiments had been performed in the PAX-El reactor configuration.

Additional evidence existed to support the niobium and molybdenum coefficients selected. A quadrant of niobium and molybdenum wires was removed from the PAX-El reactor configuration. Using the selected reactivity coefficients for molybdenum and niobium generated, it was possible to predict the reactivity effect of the wire removal within 0.4¢.

The reactivity coefficients of silver, iridium, rhodium, paladium, rhenium, and tungsten were required for determining the reactivity effect of NRX-A6 core instrumentation (thermocouples and thermal capsules). These reactivity coefficients were measured as a function of radial position in the PAX reactor which simulated the NRX-A2 reactor. These coefficients are reported in Reference 3.

The volume-average reactivity coefficients (shown in Figure 5.11) for carbon, uranium, niobium, tantalum, and molybdenum were obtained by integrating the radial reactivity coefficient curves shown in Figures 5.4 through 5.8. The reactivity coefficient of nickel was obtained on a core average basis from an experimental measurement in which nickel wires were placed uniformly over the core of the PAX-E2 reactor. The reactivity effect of hydrogen was obtained from measurements in previous NRX reactor configurations. The core average reactivity coefficients of iron and chromium were obtained from one-dimensional transport calculations which had been normalized by multiplying the calculated results by the ratio of the experimental to calculated reactivity worth of nickel. The reactivity coefficient of stainless steel was obtained from the core average reactivity coefficients given for iron, nickel, chromium. The reactivity coefficient of Inconel-718 was obtained from core average reactivity coefficient given for iron, nickel, chromium, niobium, and molybdenum.

5.2 Fuel Interchange Experiment

A quadrant of NRX-A6 pre-production fuel (A6-Q fuel) was substituted into the PAX-E1 reactor configuration. The A6-Q fuel replaced PAX-E1 fuel which had been modified to simulate the NRX-A6 uranium loading distribution, as noted earlier, by replacing fueled elements with unfueled nineteen-hole graphite elements. In this manner, the PAX reactor, which originally had a uranium loading distribution similar to the NRX-A2 reactor, was made to have a uranium loading distribution which, at least on a gross basis, was similar to the NRX-A6 loading distribution. Figure 5.12 shows the following information concerning the fuel substitution experiment:

1) The steps involved in the fuel substitution.
2) The location of the elements involved in each step of the fuel substitution.
3) The experimentally measured reactivity change for each step of the A6-Q/PAX-Q fuel substitution.

5.3 Non-Core Reactivity Coefficients

Figure 5-13 displays the reactivity coefficients which were used in determining the reactivity difference between the NRX-A6 and PAX-E1 reflector components. This figure also indicates whether the reactivity coefficient was determined from WANEF experimental data, LASL experimental data, or calculations, and which data are applicable only to materials located in radial spring holes in the reflector which are streaming paths for neutrons.

Astronuclear Laboratory

FIGURE 5.12

A6-Q/PAX-Q FUEL INTERCHANGE

EXPERIMENTAL RESULTS

Step Number	Elements Changed	Experimentally Measured Reactivity Change, ¢ A6-Q Minus PAX-Q
1	4B2 C,D,E,F 5B1 B through G 5B2 C,D,E,F 4C2 B,D,E,F,G 4C3 B through G 5C1 B through G 5C2 B through G 5C3 B,C,D,E	+7.7
2	4D2 E,F,G 4D3 B through G 4D4 B through G 5D1 B,C,F,G 5D2 B through G 5D3 B through G 5D4 C,D,E	+1.7
3	5D1 D,E 4E3 B through G 4E4 B through G 4E5 B through G 5E1 B,C,F,G 5E2 B through G 5E3 B through G 5E4 B through G 5E5 C,D 4F4 B,G 5F4 B,G	+5.6
4	5E1 D,E 4F3 B,E,F,G 4F4 C,D,E,F 4F5 B through G 4F6 B through G 5F1 B through G 5F2 B through G 5F3 B through G 5F4 C,D,E,F 5F5 B through G	+12.3

FIGURE 5.12 (Continued)

5	4G3 F,G	+7.1
	4G4 B,C,D,F,G	
	4G5 B,C,D,F,G	
	4G6 B,C,D,G	
	4G7 B,C	
	5G2 B,G	
	5G3 B,C,F,G	
	5G4 B,C,D,F,G	
	5G5 B,C,D,F,G	
	5G6 B,C,D	
6	4G3 E	+0.6
	4G4 E	
	4G5 E	
	4G6 E,F	
	4G7 D,E,F,G	
	5G1 B through G	
	5G2 C,F,D,E	
	5G3 D,E	
	5G4 E	
	5G5 E	
	5G6 E	
	4H3 F	
	4H4 B through G	
	4H5 B through G	
	4H6 B through G	
	4H7 B through G	
7	5H3 B through G	-0.3
	5H4 B through G	
	5H5 B through G	
	5H6 B through G	
	5H7 C,D,E	
	4J4 B,G	
	4J5 B,C,G	
	4J6 B,C,G	
	4J7 B,C,G	
	4J9 B,C,D,G,R,W	
	5J3 B,C,F,G	
	5J4 B,G	
	5J5 B,C,G	
	5J6 B,C,G	
	5J7 B,C,G	
8	4J4 C,D,F,H,K,M	-2.1
	4J5 D,F,H,J,K	
	4J6 D,F,H,K	
	4J7 D,F,H,K	
	4J8 B,C,D,F,G	
	4J9 E,F,H,K,P,S,T,U,V	
	5J3 D,E,H,J,N,R,S,T,U,V,W	
	5J4 C,D,F,H,K,M	
	5J5 D,F,H,J,K	
	5J6 D,F,H,K	
	5J7 D,F,H,K	
	5J8 C,D	
	TOTAL REACTIVITY CHANGE	32.6¢

FIGURE 5.13

NRX-A6

AVERAGE REACTIVITY COEFFICIENTS FOR NON-CORE REGIONS

Region	Material	Reactivity Coefficient (c/Kg)
Filler Strip	Carbon (1)	+ 3.0
	Niobium (1)	- 4.2
	Stainless Steel (1)	- 3.28
Lateral Support	Carbon (1)	+ 2.9
	Aluminum (2)	+ 0.26
Beryllium Reflector	Beryllium (1)	+ 2.2
	Carbon (1, 4)	+ 3.5
	Inconel (1, 4)	- 0.25
	Stainless Steel (3, 4)	- 0.25
	Nispan (3, 4)	- 0.25
	Titanium (3, 4)	- 2.0
	Copper (3, 4)	- 0.25
	Aluminum (1, 4)	+ 0.37
Cluster Plate	Steel (3)	+ 0.67
	Inconel (3)	+ 0.81
Support Block	Carbon (1)	+ 1.36
	Niobium (1, 2)	+ 0.41
	Stainless Steel (3)	+ 0.45
	Molybdenum (3)	+ 0.49
	Tungsten (3)	+ 0.18
	Inconel (3)	+ 0.65
Support Plate	Aluminum (1, 3)	+ 0.16

(1) Based on WANEF experimental data.
(2) Based on LASL experimental data.
(3) Based on calculations.
(4) Applicable to materials located in the radial spring hole.

The reactivity coefficients measured at WANEF for the filler strip and lateral support region were determined in the PAX-E2 reactor configuration between the NRX-A6 preproduction fuel and the NRX-A2 beryllium sectors which closely represented the NRX-A6 beryllium reflector in the distribution and mass of beryllium. The reactivity coefficients measured at WANEF for the beryllium reflector and support block region were obtained in the PAX-E0 reactor configuration. The beryllium reflector coefficients were measured opposite the NRX-A6 Build 1 fuel in the NRX-A2 beryllium sectors which closely simulated the NRX-A6 reflector. The reactivity coefficients for the cluster plate and support plate regions were measured at WANEF in a PAX reactor which simulated previous NRX reactor configurations. The method used to determine the reactivity effect of instrumentation, external structures, bundling pressure, and pressure vessel is discussed in Section 8.0.

5.4 Uncertainties in Reactivity Effects

Figure 5.14 shows the reactivity uncertainty which occurs because of uncertainties in reactivity coefficients. The statistical sum of these uncertainties was found to be $\pm 0.58\$$.

The uncertainty in a reactivity coefficient was based on the following three considerations:

1) Accuracy of the experimental measurement,

2) Accuracy of the calculation techniques used to determine or normalize certain coefficients, and

Astronuclear Laboratory

FIGURE 5.14

REACTIVITY UNCERTAINTY DUE TO REACTIVITY EFFECT UNCERTAINTIES

Region	Material	Mass Difference kg	Reactivity Coefficient & Uncertainty, ¢/kg	Reactivity Uncertainty, ¢
Core	Fueled Elements			
	Carbon	1.977	5.04 ± 0.5	± 1.0
	Uranium	8.381	15.01 ± 1.5	±12.6
	Niobium	3.024	5.55 ± 1.0	± 3.0
	Molybdenum(1)		-13.68 ± 3.0	±18.0
	Interaction Effects & Calculational Technique			±40.0
	Unfueled Elements			
	Carbon	1.201	5.04 ± 0.5	± 0.6
	Tantalum	2.751	-61.72 ± 6.2	±17.0
	Niobium	7.671	-5.55 ± 0.6	± 4.6
	Hydrogen	0.0	670.0 ±67.0	± 0.0
	Hardware			
	Positive Shims	1.017	5.04 ± 0.5	± 0.5
	Pyrographite Sleeves	0.317	5.04 ± 0.5	± 0.1
	Tie Rods	1.065	---	±15.0
	Tube Liners	-0.178	-0.24 ± 0.0	± 0.0
	Instrumentation			± 6.0
Filler Strip	Carbon	8.161	+3.0 ± 0.3	± 2.4
	Niobium	0.757	-4.2 ± 0.4	± 0.3
	Stainless Steel	-10.592	-3.28 ± 0.3	± 3.2
	Paraffin	0.0122		± 0.0
	Silicone Grease	0.0686		
Lateral Support	Carbon	4.129	+2.9 ± 0.3	± 1.2
	Niobium	0.001		± 0.0
	Aluminum	-1.975	+0.26 ± 0.0	± 0.0
Beryllium Reflector	Hardware			
	Inconel -718	0.968	-0.25 ± 0.3	±11.1
	Carbon	5.301	+3.5 ± 0.3	± 1.6
	Titanium	2.944	-2.0 ± 0.3	± 0.9
	Stainless Steel	0.691	-0.25 ± 0.3	± 0.2
	Nispan	1.986	-0.25 ± 0.3	± 0.6
	Copper	1.539	-0.25 ± 0.3	± 0.5
	Aluminum	11.929	+0.37 ± 0.3	± 3.6
	Plastic Tape	-0.326		± 0.0
	Teflon Tape	-0.156		
Reflector	Beryllium	0.0	±2.2 ± 0.2	± 0.0
	Titanium	0.0	-2.0 ± 0.2	± 0.0
Control Drums	Beryllium	0.0	+2.2 ± 0.2	± 0.0
	Aluminum	0.0	+0.37 ± 0.3	± 0.0
	Boron-10	0.0		
Cluster Plate	Ag-In-Cd	11.465	---	±10.0
	Gd Stainless Steel	-8.499	---	
	Stainless Steel	-0.02	+0.67 ± 0.1	± 0.0
	Aluminum	0.495	--- ± 0.0	± 0.0
	Inconel	0.47	+0.81 ± 0.1	± 0.0
Support Block	Carbon	-10.088	1.36 ± 0.2	± 2.0
	Niobium	7.692	0.41 ± 0.1	± 1.5
	Stainless Steel	-3.785	0.45 ± 0.1	± 0.4
	Molybdenum	0.011	0.49 ± 0.1	± 0.0
	Tungsten	4.288	0.18 ± 0.1	± 0.4
	Th O_2	0.068		± 0.0
	Inconel	1.27	0.65 ± 0.1	± 0.1
Support Plate	Aluminum	89.813	0.2 ± 0.1	± 9.0
Non-Core Instrumentation				± 1.0
External Structures				±15.0
Nozzle				± 5.0
Bundling Pressure				±10.0
Pressure Vessel				± 1.0
			Statistical Sum of Uncertainties	±58.0¢

(1) The PAX-F1 mass includes 31 and 40 mil molybdenum wires which differ in self-shielding factor from the molybdenum in NRX-A6.

3) The effect of reactivity coefficients being measured in different reactor configurations.

The data presented in Figure 5.14 also includes uncertainties for

1) The method of determining the fuel reactivity differences, and

2) The interaction effects between the PAX-E1 fuel and the NRX-A6 fuel and/or reflector.

One factor considered in the uncertainty due to interaction effects is the large reactivity anomaly which occurred when the NRX-A6 reflector rings were replaced with a mockup of the NRX-A6 reflector, i.e., the PAX-E1 reactor configuration was converted to the PAX-E2 reactor configuration. The predicted reactivity difference for this interchange was 1.5$ while the measured reactivity change was 3.2$. This represents a reactivity anomaly of 1.7$. This anomaly was considered in the interaction effect uncertainty because it is felt that the most probable cause for this anomaly is interaction effects; i.e., changes in core reactivity coefficients due to reflector changes, and vice versa.

SECTION 6.0

(CRD) NRX-A6/PAX-E1 CORE REACTIVITY DIFFERENCES

The core reactivity differences between the NRX-A6 and PAX-E1 reactors are divided into two subsections: fuel differences and nonfuel differences. The reason for this division is that the fuel differences are obtained in a manner different from the nonfuel differences.

6.1 Fuel Differences

The method of determining the reactivity difference between the NRX-A6 and PAX-E1 fuel is basically different from the reactivity estimates of previous NRX reactors. Section 3.0 described the nomenclature and outlined the conceptual reactor configurations involved in determining the reactivity difference between the NRX-A6 and PAX-E1 fuel.

The principal problem in determining the reactivity difference between the PAX-E1 and the NRX-A6 fuel is in properly utilizing the measured reactivity difference between a quadrant of NRX-A6 preproduction fuel and a quadrant of PAX-E1 fuel. Bearing this in mind, the steps in obtaining the reactivity difference between the PAX-E1 and NRX-A6 fuel were as follows:

1. The inventories of the NRX-A6 preproduction and PAX fuel in the test quadrant, identified respectively as A6-Q and PAX-Q fuel, were extrapolated to a full core (360°) inventory. These extrapolated inventories are, respectively, referred to in the text as the A6-QE and the PAX-QE fuel.
2. From these extrapolated inventories it is possible to determine the following reactivity effects by essentially

taking the product of the mass differences and the appropriate reactivity coefficient.

a. The reactivity difference between the PAX-E1 fuel and the PAX-QE fuel.

b. The reactivity difference between the NRX-A6 fuel and the A6-QE fuel.

3. The remaining item to be determined is the reactivity difference between the A6-QE and the PAX-QE fuel. This reactivity difference is in part based on the experimentally measured reactivity change between the A6-Q and PAX-Q fuel. The method for determining the reactivity difference between the A6-QE and the PAX-QE fuel is given by the formula described in Section 3.0. Basically, all this formula does is multiply the measured reactivity change for a quadrant of fuel by the calculated ratio of the reactivity effect for full core interchange of fuel to that for a quadrant of fuel. In addition, a correction factor must be applied to this result for the interaction effect which occurs between the PAX-E1 and A6-Q fuel.

4. Once the previous reactivity differences have been determined, the reactivity difference between the NRX-A6 and PAX-E1 fuel is the sum of reactivity difference between the NRX-A6 and the A6-QE fuel, the A6-QE and PAX-QE

fuel and the PAX-E1 and the PAX-QE fuel. The details of these calculations will be discussed in the following sections.

6.1.1 Method of Extrapolating Test Quadrant Data to a Full Core

The method of extrapolating the material inventory for a quadrant of fuel to a full core inventory is relatively simple; however, the method of extrapolating the reactivity effect associated with this quadrant to a full core is more complicated. To extrapolate a material inventory for a quadrant of fuel to a full core merely requires that the mass of each chemical constituent in the fuel be multiplied by the ratio of the total number of elements in the core to the number of elements in the quadrant. This extrapolation must be done for each fuel element loading code because the ratio of the number of elements in the full core to the number of elements that were in the test quadrant varies with the loading code. This occurs because the core is only perfectly symmetric on a 60° basis rather than on a 90° basis. Figures 6.1 and 6.2 give the number of elements in a full core and the number of elements in the test quadrant for A6 and PAX fuel. The A6-QE and the PAX-QE fuel inventories which were obtained from the A6-Q and PAX-Q fuel inventories are, respectively, given in Figures 6.5 and 6.4.

In determining the reactivity effect associated with a quadrant of fuel that has been extrapolated to a full core inventory, it is not only necessary to extrapolate the reactivity difference by loading code but also by position, because the reactivity effect of elements at the center of the core is considerably different than that of elements at the edge of the core.

FIGURE 6.1

RELATIVE WORTH(1) OF PAX-Q FUEL

EXTRAPOLATED TO A FULL CORE

Code and Location	Number of Elements In Quadrant	Number of Elements Full Core	Relative Reactivity Effect, ¢ In Quadrant	Relative Reactivity Effect, ¢ Full Core
04 Center	6	24	21.308	85.232
99	266	1062	1201.471	4796.850
89	7	24	22.707	77.853
79	13	48	39.678	146.503
69	9	48	25.012	133.397
59	7	24	18.248	62.565
49	7	30	16.906	72.454
39	18	72	39.864	159.456
04 Edge	50	198	108.321	428.951
Totals	383	1530	+1493.515	+5963.261

(1) This is the worth of fuel only; no Nb or Mo wire worths are included.

FIGURE 6.2

RELATIVE WORTH(1) OF A6-Q FUEL

EXTRAPOLATED TO A FULL CORE

Code and Location	Number of Elements In Quadrant	Number of Elements Full Core	Relative Reactivity Effect, ¢ In Quadrant	Relative Reactivity Effect, ¢ Full Core
18 Center	39	156	205.499	821.996
19 Center	36	144	181.255	725.020
20 Center	48	192	235.044	940.176
21	87	348	383.021	1532.084
20 Edge	13	54	49.911	207.323
19 Edge	13	48	47.878	176.780
18 Edge	15	66	52.318	230.199
17	22	78	69.941	247.973
16	21	96	60.817	278.021
15	24	84	62.518	218.813
14	12	60	28.593	142.965
13	20	72	42.330	152.388
12	7	30	13.436	57.582
11	26	102	46.419	182.105
Totals	383	1530	+1478.980	+5913.425

(1) This is the worth of fuel only; no Nb or Mo wire worths are included.

FIGURE 6.3

REACTIVITY COMPARISON BETWEEN PAX-E1[1] AND PAX-QE

(Fuel Only)

Material	PAX-QE Mass,kg	PAX-E1 Mass,kg	Mass Difference, kg	Reactivity Change, ¢ PAX-QE Minus PAX-E1
Carbon	818.065	819.298	-1.233	-8.301
Uranium	146.216	146.262	-0.046	+2.993
Niobium Coating				
Bore	58.702	58.516	+0.186	-1.588
External	0.0	0.0	0.0	
Matrix	0.0	0.0	0.0	
Wires				
Molybdenum	14.741	14.741	0.0	0.0
Niobium	17.914	17.914	0.0	0.0
Molybdenum Coating	0.0	0.0	0.0	0.0
			Total Reactivity Difference	-6.896

(1) NRX-A3 production code 89's which were used to simulate NRX-A6 code 18's are removed from this estimate.

FIGURE 6.4

REACTIVITY COMPARISON BETWEEN A6-Q AND PAX-Q

(Fuel Only)

Material	A6-Q Mass, kg	PAX-Q Mass, kg	Mass Difference kg	Reactivity Change, ¢ A6-Q Minus PAX-Q
Carbon	204.314	204.784	-0.470	-1.539
Uranium	39.010	36.626	2.384	+30.828
Niobium Coating				
Bore	19.042	14.667	4.375	-18.406
External	0.553	0.0	0.553	-2.076
Matrix	0.0	0.0	0.0	0.0
Wires				
Molybdenum	0.0	3.720	-3.720	+23.148
Niobium	0.0	4.582	-4.582	+20.490
Molybdenum Coating	1.713	0.0	1.713	-23.342
			Total Reactivity Difference	+29.103

FIGURE 6.5

REACTIVITY COMPARISON BETWEEN A6-QE(1) AND PAX-CE

(Fuel Only)

Material	A6-QE Mass, Kg	PAX-QE Mass, kg	Mass Difference, Kg	Reactivity Change, ¢ A6-QE Minus PAX-QE
Carbon	816.221	818.065	-1.844	-1.888
Uranium	156.004	146.216	9.788	+126.175
Niobium Coating				
Bore	75.847	58.702	17.145	-72.58
External	2.130	0.0	2.130	-7.933
Matrix	0.0	0.0	0.0	0.0
Wires				
Molybdenum	0.0	15.248	-15.248	+91.73
Niobium	0.0	18.077	-18.077	+80.11
Molybdenum Coating	6.901	0.0	6.901	-93.558
			Total Reactivity Difference	+122.056

(1) 54 code 18's from center were removed from this estimate for consistency.

This refinement in the reactivity extrapolation is demonstrated in Figure 6.1 by the code 04 elements in the PAX-Q fuel.

Figures 6.1 and 6.2 display, respectively, the net relative reactivity effects of the PAX-Q and A6-Q fuel. These results for the A6-Q and PAX-Q fuel were obtained from the AMDS computer code.

The net relative reactivities reported in Figures 6.1 and 6.2 are the sum of the products of the total mass of each chemical constituent in the fuel and the appropriate reactivity coefficient. This quantity is purely a mathematical entity and has no relation to reactivity in the physical sense; however, the difference in the two numbers thus obtained represents the reactivity difference between the two sets of fuel inventories.

These net relative reactivity effects could not be made representative of a physical reactivity difference because of the extrapolation process involved with this fuel and the inherent limitations of the AMDS computer program. For example, to make the reactivities reported in these tables have a meaning in a physical sense, it would have been necessary to supply some base case on which the reactivity difference could be determined. However, the reactivity calculations were performed for a quadrant of fuel and then extrapolated to a full core. This means that any base case employed to give the net relative reactivities some physical meaning would had to have also been extrapolated to a full core inventory. Since the extrapolation ratio for the A6-Q and PAX-Q fuel is not the same, the base case in the PAX-QE fuel would have been different from the base case in the A6-QE fuel. This would result in a reactivity discrepancy between the A6-QE and PAX-QE fuel.

The above method of extrapolating the reactivity effect of a quadrant of fuel to the reactivity effect of a full core has been verified through the use of the AMDS computer code. Due to the inherent limitations of the AMDS computer program, it was not possible to perform this extrapolation in the same manner. The results obtained by the AMDS program gave an extrapolated net relative reactivity effect which agreed with the extrapolations presented in Figures 6.1 and 6.2 within 0.01$. However, because the method used by the AMDS computer program to extrapolate the net relative reactivity effect is not precise, the data presented in Figures 6.1 and 6.2 are considered to be the more accurate results.

6.1.2 Reactivity Difference Between PAX-E1 Test Quadrant Extrapolation and PAX-E1 Fuel

Figure 6.3 displays the following information:

1. The mass of the fuel in the PAX-E1 reactor.
2. The mass inventory of the PAX-Q fuel extrapolated to the inventory of the PAX-QE fuel.
3. The reactivity and mass differences between the PAX-E1 fuel and the PAX-QE fuel.

This table indicates that the net reactivity difference between PAX-QE and the PAX-E1 fuel is -6.9¢. It should be noted that Figure 6.3 does include the reactivity effect of the 54, A3-C elements in the keyhole because this fuel did not change between the PAX-E1 core and the hypothetical PAX-QE core.

The relative reactivity effect for each chemical constituent of the PAX-E1 fuel was obtained by the AMDS code. The extrapolated relative

reactivity effect for the PAX-QE fuel was obtained in the previous section. The reactivity difference between the PAX-E1 fuel and PAX-QE fuel is then the difference between these two relative reactivity effects.

The reactivity difference of -6.9¢ between the PAX-QE and PAX-E1 fuel is due primarily to the mass of carbon in the code 04 elements located in the test quadrant. It was discovered that some of the code 04 elements in the test quadrant contained on the average approximately 20 grams less graphite than the remaining code 04 elements. This decrease in the carbon mass of some of the code 04 elements in the test quadrant is extrapolated to a full core thus resulting in a reactivity difference between the PAX-E1 and PAX-QE fuel of approximately 5¢. The remaining reactivity difference between PAX-E1 and PAX-QE fuel is due only to statistical variations in the fuel content.

6.1.3 Reactivity Difference Between the NRX-A6 Test Quadrant Extrapolation and the PAX-E1 Test Quadrant Extrapolation Fuel

The calculated reactivity difference between the A6-Q and PAX-Q fuel is 29.1¢, and that calculated between the A6-QE and PAX-QE fuel is 122.1¢, as shown in Figures 6.4 and 6.5. The reactivity difference between the A6-QE and PAX-QE fuel based on the quadrant fuel substitution experiment is 135.2¢, and the calculation is shown in Figure 6.6.

The fuel inventories, mass differences, and reactivity differences shown in Figures 6.4 and 6.5 were determined in a manner similar to that in which the reactivity difference between the PAX-E1 and PAX-QE fuel was determined in the previous section. Neither of these calculations include the 54, A3-C, elements located at the center of the core because this fuel

FIGURE 6.6

REACTIVITY DIFFERENCE BETWEEN

A6-QE AND PAX-QE FUEL BASED

ON THE FUEL INTERCHANGE EXPERIMENT

$$\rho_{(A6\text{-}QE/PAX\text{-}QE)} = \rho \times \frac{\rho_{(A6\text{-}QE/PAX\text{-}QE)^{Calc.}}}{\rho_{(A6\text{-}Q/PAX\text{-}Q)^{Calc.}}}$$

where the definitions of the above terms are given in Section 3.0.

ρ = 32.6 ¢ (See Figure 5.12)

$\rho_{(A6\text{-}QE/PAX\text{-}QE)^{Calc.}}$ = 122.056¢ (See Figure 6.5)

$\rho_{(A6\text{-}Q/PAX\text{-}Q)^{Calc.}}$ = 29.103¢ (See Figure 6.4)

$$\rho_{(A6\text{-}QE/PAX\text{-}QE)} = 32.6¢ \times \frac{122.056}{29.103}$$

$$= 136.6¢$$

The following is a correction for interaction effects.

$$\rho_{(A6\text{-}QE/PAX\text{-}QE)} = 136.64 \times \frac{3.959}{4.0} = 135.2¢$$

has not changed. It should be noted that the experimentally measured reactivity difference obtained for the quadrant substitution is 32.6¢ which is in excellent agreement with the calculated value of 29.1¢.

Applying the formula given in Section 3.0, the reactivity difference between the A6-QE and and PAX-QE fuel based on the quadrant interchange experiment was found to be 136.6¢ (See Figure 6.6 for details). This reactivity difference between the A6-QE and PAX-QE fuel does not take into account the interaction effects which occurred when the A6-Q fuel was substituted into the PAX-E1 reactor. A series of three R - Θ geometry, diffusion theory calculations were performed to determine the interaction effect. The three diffusion theory calculations modeled the PAX-E1 mockup of the NRX-A6 reflector with the following core configurations:

1. A full core (360°) of PAX-E1 fuel.
2. A full core (360°) of A6-QE fuel.
3. A core which contained 270° of PAX-E1 fuel and the 90° of A6-Q fuel.

The reactivity difference between the first and second problem gave the reactivity change which would occur for a complete core substitution of A6-QE fuel for PAX-E1 fuel. The reactivity difference between the first problem and the third problem gave the reactivity difference which would occur for a quadrant substitution of A6-Q fuel for PAX-Q fuel.

It was found that the reactivity effect of a complete core substitution was only 3.959 times the reactivity effect of a single quadrant substitution. This indicates that the experimentally measured reactivity effect was slightly too high. This result can be understood if one relates this problem to a similar one which is often encountered in control rod theory; namely, the reactivity effect of the first control rod inserted into a core is greater than that of a second control rod inserted into the core.

The neglect of the interaction effect would cause the previously derived reactivity difference between A6-QE and PAX-QE fuel in the previous paragraph to be slightly high. Therefore, this reactivity difference should be reduced by (3.959/4.000 =) 0.9898. Applying this factor to the previous calculation, the calculated reactivity difference between the A6-QE and PAX-QE fuel becomes 135.2¢.

As can be seen from Figure 6.5, a large reactivity difference between the A6-QE and PAX-QE fuel is due to the niobium and molybdenum coating. This difference occurs because the PAX-QE fuel did not contain a molybdenum coating and did not contain a niobium coating as heavy as that on the A6-QE fuel. However, these differences in coatings were corrected by the use of niobium and molybdenum wires. Figure 6.5 indicates that the wires effectively counterbalance the reactivity differences due to the coatings.

Figure 6.5 indicates that the major reactivity difference between the A6-QE and the PAX-QE fuel is due to uranium. The difference in the uranium content occurs because the A6-QE fuel contains loading code 21 fuel elements which have 140 grams of uranium per element. On the other hand, the maximum loading in the PAX-QE fuel is approximately 123 grams per element.

This difference in inventory occurred because there was no fuel available for PAX which had a uranium loading sufficiently high to match that of the A6-QE code 21 fuel. Since the A6-QE fuel contains 348 code 21 elements, the inventory difference noted above would account for approximately 6 kgs of the difference in uranium between the A6-QE and PAX-QE fuel. The remaining difference occurs because the A6-QE fuel loading distribution was not exactly simulated by the insertion of code 04 unfueled elements for fueled elements.

6.1.4 Reactivity Difference Between NRX-A6 Test Quadrant Extrapolation and NRX-A6 Fuel

Figure 6.7 shows the fuel inventories, mass differences and reactivity differences between the NRX-A6 and A6-QE fuel. The reactivity difference between the NRX-A6 and A6-QE fuel is -12.7¢. This reactivity difference was derived in a manner similar to that described in Section 6.1.2 where the reactivity difference between the PAX-QE and PAX-E1 fuel was determined. It should be noted that the reactivity comparisons given in Sections 6.1.2 and 6.1.3 did not include the centermost 54 elements (A3-C fuel) of the core whereas the reactivity difference in this section does.

From Figure 6.7, it can be seen that the major reactivity difference between the NRX-A6 and A6-QE fuel occurs because the NRX-A6 fuel contained experimental elements with niobium added to the fuel matrix. The other reactivity differences between the NRX-A6 and A6-QE fuel are small and due to statistical variation in the fuel.

6.1.5 Summary of the Reactivity Differences Between the NRX-A6 and PAX-E1 Fuel

The reactivity difference between the PAX-QE fuel and the PAX-E1

FIGURE 6.7

REACTIVITY DIFFERENCE BETWEEN NRX-A6 AND A6-QE

(Fuel Only)

Material	NRX-A6 Mass, kg	A6-QE Mass, kg	Mass Difference kg	Reactivity Change, ¢, NRX-A6 Minus A6-QE
Carbon				
Non-Keyhole Fueled(1)	817.505	816.221	1.100	+4.294
Keyhole Fueled(1)	28.786	28.970		
Uranium				
Non-Keyhole Fueled	154.431	156.004	-1.359	-8.480
Keyhole Fueled	5.957	5.743		
Niobium Coating				
Bore				
Non-Keyhole	75.911	75.847	0.073	-6.676
Keyhole	2.658	2.649		
External				
Non-Keyhole	1.572	2.130	-0.558	+2.043
Keyhole				
Matrix	2.125	0.0	2.125	-11.8
Molybdenum Coating				
Non-Keyhole	6.469	6.901	-0.196	+1.604
Keyhole	0.236	0.0		
Wires(2)				
Molybdenum	0.0	0.507	-0.507	+4.998
Niobium	0.0	0.163	-0.163	+1.320
			Total Reactivity Difference	-12.697

(1) The keyhole is identified as the 54 elements in the center of the core (A3-C fuel in PAX-E1).
(2) Wires located in keyhole only.

fuel was obtained in Section 6.1.2 and found to be -6.9¢. The reactivity difference between the PAX-QE fuel and the A6-QE fuel is derived in Section 6.1.3 and was found to be 135.2¢. The reactivity difference between the A6-QE fuel and the NRX-A6 fuel was derived in Section 6.1.4 and was found to be -12.7¢. The total reactivity difference between NRX-A6 and PAX-E1 fuel is the sum of these three reactivity differences, which is 115.6¢. These results are summarized in Figure 6.8.

6.2 NRX-A6/PAX-E1 Non-Fuel Differences

6.2.1 Central Support Elements

Figure 6.9 shows the reactivity difference between the unfueled elements in the NRX-A6 and PAX-E1 reactor. This reactivity difference is -194.6¢ and was determined in the traditional manner by applying reactivity coefficients to mass differences. The large difference in reactivity between the NRX-A6 and PAX-E1 unfueled elements occurs primarily because the NRX-A6 unfueled elements contain 38 TaC-loaded negative shim elements whereas the PAX-E1 unfueled elements contain only one of these elements.

An additional negative reactivity change occurs because the NRX-A6 unfueled elements had considerably more niobium coating than the PAX-E1 unfueled elements. The NRX-A6 unfueled central support elements typically contain 7 grams of niobium deposited along the bores and 21 grams of niobium deposited on the external surfaces of the element.

The PAX-E1 central support elements were originally part of the NRX-A2 production of fuel. Therefore, the central support unfueled elements in PAX-E1 contained no niobium coating in the bores or on the external surfaces.

FIGURE 6.8

SUMMARY OF THE REACTIVITY DIFFERENCES

BETWEEN NRX-A6 AND PAX-E1 FUEL

ρ (PAX-QE Minus PAX-E1)	= -6.896¢
ρ (A6-QE Minus PAX-QE)	= 135.238¢
ρ (NRX-A6 Minus A6-QE) + ρ (NRX-A6 Minus A3-C)	= -12.697¢
Total ρ (NRX-A6 Minus PAX-E1)	= +115.645¢

FIGURE 6.9

NRX-A6 AND PAX-E1 CORE REACTIVITY DIFFERENCES

Material	NRX-A6 Mass Kg	PAX-E1 Mass Kg	Mass Difference Kg	Reactivity Change, ¢ NRX-A6 Minus PAX-E1
Fueled Elements				
Carbon	846.291	848.268	1.977	
Uranium[1]	160.388	152.007	8.381	
Niobium[2]				
Bore	78.569	79.242	-0.673	
External	1.572	0.0	1.572	
Molybdenum[2]	6.705	15.248	See Note 3	
Total for above items				127.5
Matrix Niobium	2.125	0.0	2.125	-11.8
			Fueled Subtotal	115.7
Unfueled Elements				
Carbon	195.925	194.724	1.201	4.0
Tantalum	2.826	0.075	2.751	-155.8
Niobium[2]				
Bore	2.014	0.008	2.006	-10.9
External	5.954	0.289	5.665	-31.9
			Unfueled Subtotal	-194.6
Hardware				
Positive Shims	1.017	0.0	1.017	5.1
Pyrographite Sleeves	27.413	27.730	-0.317	-1.7
Tie Rods[4]	23.647	22.582	1.065	-20.0
Tube Liners	8.044	8.222	-0.178	0.1
Instrumentation				-19.6
			Hardware Subtotal	-36.1
			Total Core Reactivity Difference	-115.0

(1) Mass of uranium adjusted to 52 inches.

(2) Reactivity - weighted mass.

(3) The PAX-E1 mass includes 31 and 40 mil molybdenum wires which differ in self-shielding factor from the molybdenum NRX-A6

(4) The PAX-E1 tie rods are stainless steel while the NRX-A6 tie rods are Inconel-718.

The only unfueled elements in the PAX-El reactor which had a significant amount of niobium were the unfueled partial elements (code 03) which had their external surfaces coated with approximately 7 grams of niobium.

6.2.2 Instrumentation

There was no instrumentation in the core of PAX-El reactor. The core region of NRX-A6 contained 64 thermocouples and 81 thermal capsule families. Figure 2.1 shows the radial placement of instrumentation in NRX-A6. The core instrumentation differences between NRX-A6 and PAX-El are summarized in Figure 6.10 which indicates that the sum of these differences is approximately -0.20$.

The reactivity of these instruments was obtained by determining the reactivity coefficient of the materials in the instrument at the instruments' radial position. The product of these reactivity coefficients and the sine-squared weighted masses of the materials in the instrument gave the reactivity associated with the instrument.

Reactivity coefficients for Ag, Ir, Pd, Rh, Re, Ta, and W were obtained from WANEF measurements. These elements contributed approximately 80 percent of the reactivity effect in the thermal capsules and approximately 60 percent of the reactivity effect in the thermocouples.

The reactivity coefficients of the other instrument constituents (Al, Au, Be, Cu, Cr, Pt, Mo, and Mg) were derived from reactivity coefficients measured in the PPA reactor series (See Reference 2). The reactivity coefficients of these constituents were assumed to follow the measured radial dependence of Ta.

FIGURE 6.10

REACTIVITY WORTH OF CORE INSTRUMENTATION

INSTRUMENT	NUMBER OF INSTRUMENTS		WORTH OF INSTRUMENTS (¢)		REACTIVITY DIFFERENCE (¢)
	NRX-A6	PAX-E1	NRX-A6	PAX-E1	
Thermocouple	64	0	-5.89	0	-5.89
Thermal Capsule Family	81	0	-13.69	0	-13.69
				Total	-19.58

The core instrumentation summary, thermal capsule specification and the thermal capsule distribution in the core and hot buffer filler strips are given in Reference 4.

6.2.3 Core Hardware

Figure 6.9 shows the reactivity difference between NRX-A6 and PAX-E1 core hardware. This reactivity difference is -0.36$ and was obtained by application of reactivity coefficients to the mass differences.

Figure 6.9 indicates that the NRX-A6 reactor contained 1.017 kgs of positive shims, whereas the PAX-E1 reactor contained no positive shims. An explanation of this result is in order. The mass of the positive shims in the NRX-A6 reactor includes the carbon due to positive shims, thermal capsules and graphite plugs which are located aft of the thermocouples. The PAX-E1 reactor had a number of positive shims in the core; however, the mass of these positive shims was not obtained explicitly because the inventory information for the PAX-E1 unfueled elements supplied by WANEF gave only the total mass of the element including the positive shim mass.

Figure 6.9 shows the reactivity difference between the NRX-A6 and PAX-E1 tie rods to be -20.0¢ but a mass difference of only 1.067 kg. This occurs because the NRX-A6 tie rods were made of Inconel-718 while the PAX-E1 tie rods were made of stainless steel.

The PAX-E1 tie rods are primarily an iron-nickel-chromium composition; the NRX-A6 tie rods are of an iron-nickel-chromium composition which has a

higher percentage of nickel than stainless steel and contains appreciable amounts of niobium and molybdenum. An examination of the core-average reactivity coefficients given in Section 5 (Figure 5.8) indicates that niobium, molybdenum, and nickel have a considerably higher reactivity effect than does iron or chromium. This is the reason for the core-average reactivity coefficient of Inconel-718 being -1.21¢/kg while the core-average reactivity coefficient of stainless steel is -0.24¢/kg.

6.3 Summary of NRX-A6 and PAX-El Core Reactivity Differences

Figure 6.9 displays the core reactivity difference between the NRX-A6 and PAX-El reactors. It was found that the NRX-A6 fuel was 1.16$ more reactive than the PAX-El fuel. In addition, it was found that the NRX-A6 unfueled elements were 1.95$ less reactive than the PAX-El unfueled elements. Finally, it was determined that the NRX-A6 core hardware was 0.36$ less reactive than the PAX-El core hardware. These reactivity differences resulted in a net reactivity difference between the NRX-A6 and PAX-El core of -1.15$.

SECTION 7.0

(CRD) NRX-A6/E1 NON-CORE REACTIVITY DIFFERENCES

The non-core reactivity differences between the NRX-A6 and PAX-E1 reactors are summarized in Figure 7.1 which indicates that the sum of these differences (Subtotal A) is 0.79$. For the most part, these reactivity differences were obtained by the application of reactivity coefficients to the mass difference between the NRX-A6 and PAX-E1 reactor. The following subsections describe in more detail how the reactivity effects were obtained. Section 8.0 describes the non-core reactivity effects which are not determined in the manner indicated above.

7.1 Filler Strip and Lateral Support Region Differences

Figure 7.1 indicates that the NRX-A6 filler strip region is 0.57$ more reactive than the PAX-E1 filler strip region. This reactivity difference is due to the following two differences between NRX-A6 and PAX-E1:

1) The NRX-A6 filler strip region contains a grafoil friction plane and impedance wrapper, filler strips and the pyrographite tiles; whereas, the PAX-E-1 filler strip region contains only a filler strip. The NRX-A6 pyrographite tiles have a higher density (2.14 g/cc) than did the corresponding section of material in the PAX-E1 filler strip region (1.84 g/cc).

FIGURE 7.1

NRX-A6/PAX-E1 NON-CORE REACTIVITY DIFFERENCES

Region	Material	NRX-A6[1] Mass, Kg	PAX-E1[1] Mass, Kg	Difference Kg	Reactivity Coefficient, ¢/Kg	Reactivity Change, NRX-A6 Minus PAX-E1, ¢
Filler Strip	Carbon	95.481	87.32	8.161	+ 3.0	24.5
	Niobium	0.757	0.0	0.757	- 4.2	-3.2
	Stainless Steel	0.0	10.592	-10.592	- 3.28	34.7
	Paraffin	0.0122	0.0	0.0122		1.0
	Silicone Grease	0.0686	0.0	0.0686		
Lateral Support	Carbon	115.082	110.953	4.129	+ 2.9	12.0
	Niobium	0.001	0.0	0.001		0.0
	Aluminum	0.0	1.975	-1.975	+ 0.26	-0.5
Beryllium Reflector Hardware	Inconel-718	37.109	36.141	0.968	- 0.25	-0.2
	Carbon	5.301	0.0	5.301	+ 3.5	18.6
	Titanium	2.944	0.0	2.944	- 2.0	-5.9
	Stainless Steel	0.691	0.0	0.691	- 0.25	-0.2
	Nispan	1.986	0.0	1.986	- 0.25	-0.5
	Copper	1.539	0.0	1.539	- 0.25	-0.4
	Aluminum	11.929	0.0	11.929	+ 0.37	4.4
	Plastic Tape	0.0	0.326	-0.326		~0.0
	Teflon Tape	0.0	0.156	-0.156		~0.0
Reflector	Beryllium	884.5	884.5	0.0	2.2	0.0
	Titanium	14.67	14.67	0.0		0.0
Control Drums	Beryllium	199.85	199.85	0.0	2.2	0.0
	Aluminum	18.111	18.111	0.0		0.0
	Boron-10	1.0283	1.0283	0.0		0.0
Cluster Plate	Ag-In-Cd	11.465	0.0	11.465		-10.0
	Gd Stainless Steel	0.0	8.499	-8.499		0.0
	Stainless Steel	20.32	20.3	0.02	0.67	0.0
	Aluminum	2.49	1.995	0.495		0.0
	Inconel	0.52	0.04	0.47	0.81	0.4
Support Block	Carbon	27.525	37.613	-10.088	1.36	-13.7
	Niobium	7.692	0.0	7.692	0.41	3.1
	Stainless Steel	0.21	3.995	-3.785	0.45	-1.7
	Molybdenum	1.47	1.459	0.011	0.49	0.0
	Tungsten	4.288	0.0	4.288	0.18	0.8
	ThO_2	0.068	0.0	0.068		~0.0
	Inconel	1.27	0.0	1.27	0.65	0.8
Support Plate	Aluminum	212.285	122.472	89.813	0.2	14.5
					Non-Core Subtotal A	78.5

Material	NRX-A6 Worth, ¢	PAX-E1 Worth, ¢	Reactivity Change NRX-A6 Minus PAX-E1, ¢
Instrumentation			
Flame Sprayed Instrumentation Leads	1.6	0.0	1.6
Thermocouples	-0.4	0.0	-0.4
Thermal Capsules	-2.9	0.0	-2.9
Resistance Thermometers	-0.1	0.0	-0.1
External Structures	21.0	21.8	-0.8
Nozzle	18.3	0.0	18.3
Bundling Pressure	19.9	0.0	19.9
Pressure Vessel	2.9	0.0	2.9
		Non-Core Subtotal B	38.5
		Non-Core Total	117.0

[1] Mass adjusted to 52.0 inches.

2) The PAX-E1 reactor contained a 10 kg stainless steel, lateral support bundling mechanism which was not present in the NRX-A6 reactor. This stainless steel bundling mechanism in PAX-E1 resulted in a 0.35$ negative reactivity insertion for the PAX-E1 reactor, thus making NRX-A6 more reactive.

Figure 7.1 indicates that the NRX-A6 lateral support region is 0.12$ more reactive than the PAX-E1 lateral support region. This difference occurs because the PAX-E1 mockup of the NRX-A6 lateral support was 4 kgs different than the NRX-A6 lateral support region mass. The NRX-A6 lateral support contained inner and outer seal segments, and an insulating tile; whereas, the PAX lateral support region contained only graphite liner plates which approximated the A6 lateral support. In addition, the PAX-E1 lateral support included an aluminum container which could be employed for emergency shutdown procedures.

The carbon reactivity coefficient in the lateral support region was obtained by inserting graphite rods in the lateral support and noting the reactivity effect which resulted. In addition, reject NRX-A6 inner and outer seal segments were attached to a PAX-E2 beryllium liner plate. The resulting configuration closely approximated the actual NRX-A6 lateral support region. The reactivity coefficient obtained from this measurement was found to be similar to that obtained in the graphite rod measurement when the axial distribution of the seal segments had been taken into account.

7.2 Beryllium Reflector Differences

Figure 7.1 shows the reactivity differences between the NRX-A6 and PAX-E1 beryllium reflector regions. It was found that the NRX-A6 beryllium reflector region was 0.16$ more reactive than the PAX-E1 beryllium reflector region. As can be seen from Figure 7.1, no differences in reactivity between NRX-A6 and PAX-E1 resulted due to the beryllium reflector rings or the control drums.

The lateral support hardware reactivity coefficients were found by inserting materials in the radial spring holes. Because the spring holes are radial streaming paths for neutrons, it was found that moderating materials had a larger positive reactivity effect and that absorbing materials had a smaller negative reactivity effect. The reactivity coefficients measured in PAX-E0 for the lateral support hardware had to be adjusted slightly because the coefficients showed a marked dependence upon azimuthal location, and the spring holes located in the PAX-E0 reactor configuration were not at exactly the same azimuthal locations as those in the NRX-A6 reflector. In addition, it should be noted that reactivity coefficients for the iron, nickel, chromium, and copper alloys in the spring hardware were not explicitly obtained. The reactivity coefficient of -0.25¢/kg was obtained for Inconel 600. A comparison of the macroscopic scattering and absorption cross sections for the other alloys located in spring holes indicated that these materials had similar cross sections. Therefore, the reactivity effect of these metallic spring hardware components were assumed to be the same as that measured for Inconel 600.

7.3 Support Block Differences

Figure 7.1 indicates that the NRX-A6 support block region is 0.11$ less reactive than the PAX-E1 support block region. The NRX-A6 reactor employed the skirtless support block design whereas the PAX-E1 reactor did not. Therefore, the NRX-A6 support blocks contained 10 kg less carbon than the PAX-E1 support blocks. This is the primary cause of the NRX-A6 loss of reactivity in the support block region.

The carbon reactivity coefficient in the support block region was measured in the PAX-E0 reactor configuration by placing hexagonal-shaped graphite pieces, 0.75 inches in length, on the PAX support blocks. The remaining reactivity coefficients in this region were measured in the NRX-A2 PAX configuration and are reported in Reference 3.

7.4 Cluster Plate and Support Plate Differences

Figure 7.1 indicates that the NRX-A6 cluster plate region is approximately 0.10$ less reactive than the PAX-E1 cluster plate region. The NRX-A6 reactor employed Ag-In-Cd cluster plates, whereas, the PAX-E1 reactor employed Gd-stainless steel cluster plates. This is the primary reason for this reactivity difference between the NRX-A6 and PAX-E1 reactors.

The reactivity effect of the two types of cluster plates was measured in the NRX-A4 PAX reactor configuration by placing the two different types of cluster plates on the support blocks of the PAX reactor. Considerable additional analysis was required to derive the reactivity effect. The results of this analysis are reported in Reference 1. The remaining reactivity coefficients in this region were obtained from LASL

measurements and one-dimensional transport calculations normalized to the LASL measurements. The results and details of this analysis are reported in Reference 3.

Figure 7.1 indicates that the NRX-A6 support plate is 0.15$ more reactive than the PAX-E1 support plate. The primary reason for this difference is that the NRX-A6 employed a flat support plate which has smaller flow holes than the support plate in PAX-E1. These changes in the support plate resulted in the NRX-A6 support plate being 90 kgs heavier than the PAX-E1 support plate. The aluminum reactivity coefficient for this region was measured in the NRX-A4 PAX reactor configuration and is reported in Reference 5. This coefficient was measured on top of the support blocks in PAX with a simulated support plate present; however, the simulated shield, which consists of 800 kgs of aluminum, was not present for the measurements. This reactivity coefficient was modified to account for the following two items:

1) A portion of the large mass difference between the the two support plates was in the corner regions of the plates.

2) One-dimensional transport calculations were performed to account for the simulated shield which was not present in the measurement.

SECTION 8.0

(CRD) ADDITIONAL REACTIVITY EFFECTS WHICH OCCURRED BETWEEN NRX-A6 AND PAX-E1

This section describes reactivity differences which occurred between NRX-A6 and PAX-E1 which could not be handled by applying a reactivity coefficient to a mass difference.

8.1 Reactivity Effect of Instrumentation

Figure 8.1 gives the reactivity worth of the instrumentation outside the core region. The NRX-A6 non-core instrumentation included 46 thermocouples, 12 thermal capsule families, 6 thermometers and the instrumentation leads which were flame-sprayed onto the wall of the pressure vessel; whereas, the PAX-E1 reactor did not contain any non-core instrumentation. This difference in instrumentation resulted in the NRX-A6 being 0.02$ less reactive than the PAX-E1 reactor.

The worth of this instrumentation was calculated in the same manner as that in the core (See Section 6.2.2). Material reactivity coefficients used in the calculattons (with the exception of the flame-sprayed lead calculations) were based on the WANEF measured coefficient of 348 stainless steel. The reactivity effect of flame-spraying the leads onto the pressure vessel wall with aluminum oxide was calculated using a measured reactivity coefficient for aluminum (See Reference 5) and a calculated coefficient for stainless steel.

FIGURE 8.1

REACTIVITY WORTH OF NON-CORE INSTRUMENTATION

ITEM	NUMBER OF ITEMS		WORTH OF ITEMS (¢)		REACTIVITY DIFFERENCE (¢)
	NRX-A6	PAX-E1	NRX-A6	PAX-E1	
Thermocouples	46	0	-0.34	0	-0.34
Thermal Capsule Family	12	0	-2.86	0	-2.86
Thermometers	6	0	-0.15	0	-0.15
Flame Sprayed Instrument Leads	-	-	-1.60	-	+1.60
				Total	-3.35

All of the constituent materials in the leads were assumed to be stainless steel. This assumption is warranted by the fact that the magnitude of the reactivity of the leads was small.

Reference 4 gives the reflector instrumentation summary and thermal capsule distribution in the filler strip region.

8.2 Reactivity Effect of External Structures

Figure 7.1 indicates that the structures external to the NRX-A6 were 0.01$ less reactive than the structures external to the PAX-El reactor. The structures external to the NRX-A6 reactor consisted of the test car and Test Cell "C" shield. The structures external to the PAX-El reactor consisted of the two test cell walls nearest the PAX reactor, the polyethylene-covered neutron detectors, and the steel support structure surrounding PAX-El. In these calculations, the materials below the dome end of the reactor (both reactors have the nozzle in the upward direction) were considered to have the same reactivity effect on each reactor.

The reactivity effect of the Test Cell "C" shield was based on a measurement made by LASL on the PARKA reactor which indicated a reactivity effect of 27.3¢ for the aluminum shield filled with 2.0 w/o borated water. The geometrical configuration of the LASL mockup of the Test Cell "C" shield was the same as for the NRX-A6 reactor; therefore, it was only necessary to take into account the effect of the differences in the NRX-A6 and PARKA reactors on the worth of the Test Cell "C" shield. This was accomplished by performing one-dimensional transport calculations for the PARKA and NRX-A6

reactors with the appropriate shield surrounding each reactor. The ratio of these two worths was applied to the experimentally measured value to obtain the calculated worth of the NRX-A6 shield which was 0.21$.

The reactivity effect of the test cell walls near the PAX-El reactor was determined in the following manner:

1) The reactivity effect of the walls was determined from a one-dimensional, infinite cylinder, radial transport calculation.

2) The fraction of the number of neutrons leaving the reactor which hit the test cell wall and return was determined by solid angle calculations.

3) The fraction of the number of neutrons which leave the reactor and return for the infinite cylinder case was determined by solid angle calculations.

4) The reactivity effect of the test cell walls was taken to be the product of a calculated worth and the ratio of the fraction of number of neutrons leaving the reactor which return in the actual case to the fraction of the number of neutrons leaving the reactor which return for the infinite cylinder case.

These calculations indicated that the test cell walls were worth 0.10$ in reactivity.

The reactivity effect of the polyethylene-covered neutron detectors was determined by a measurement at WANEF. This measurement indicated

that the six neutron detectors were worth 0.05$. The remaining 0.07$ in reactivity was attributed to the stainless steel support structure surrounding the PAX-E1 reactor.

8.3 Reactivity Effect of Bundling Pressure

Figure 7.1 indicates that the NRX-A6 reactor is 0.20$ more reactive than the PAX-E1 reactor due to bundling pressure. Under ambient conditions, the NRX-A6 reactor had a lateral support bundling pressure of 3.2 psi while the PAX-E1 reactor had a bundling pressure of 0.33 psi. Therefore, the NRX-A6 gains reactivity because the NRX-A6 core is more tightly bundled than the PAX core.

Figure 8.2 shows the reactivity effect of bundling pressure as inferred from LASL measurements (See References 3 and 6). Once the bundling pressure of the reactors is known, the reactivity difference due to the difference in bundling pressure is then obtained from Figure 8.2.

8.4 Reactivity Effect of Pressure Vessel

Figure 7.1 indicates that the NRX-A6 is 0.03$ more reactive than the PAX-E1 reactor due to a difference in the pressure vessels. The NRX-A6 pressure vessel is composed of an alloy which is 94 w/o aluminum and 6 w/o copper. The pressure vessel used on the PAX-E1 reactor is composed entirely of aluminum.

The reactivity of the PAX pressure vessel was determined experimentally to be 0.30$ in the NRX-A2 configuration of the PAX reactor.

FIGURE 8.2 REACTIVITY EFFECT OF RADIAL BUNDLING

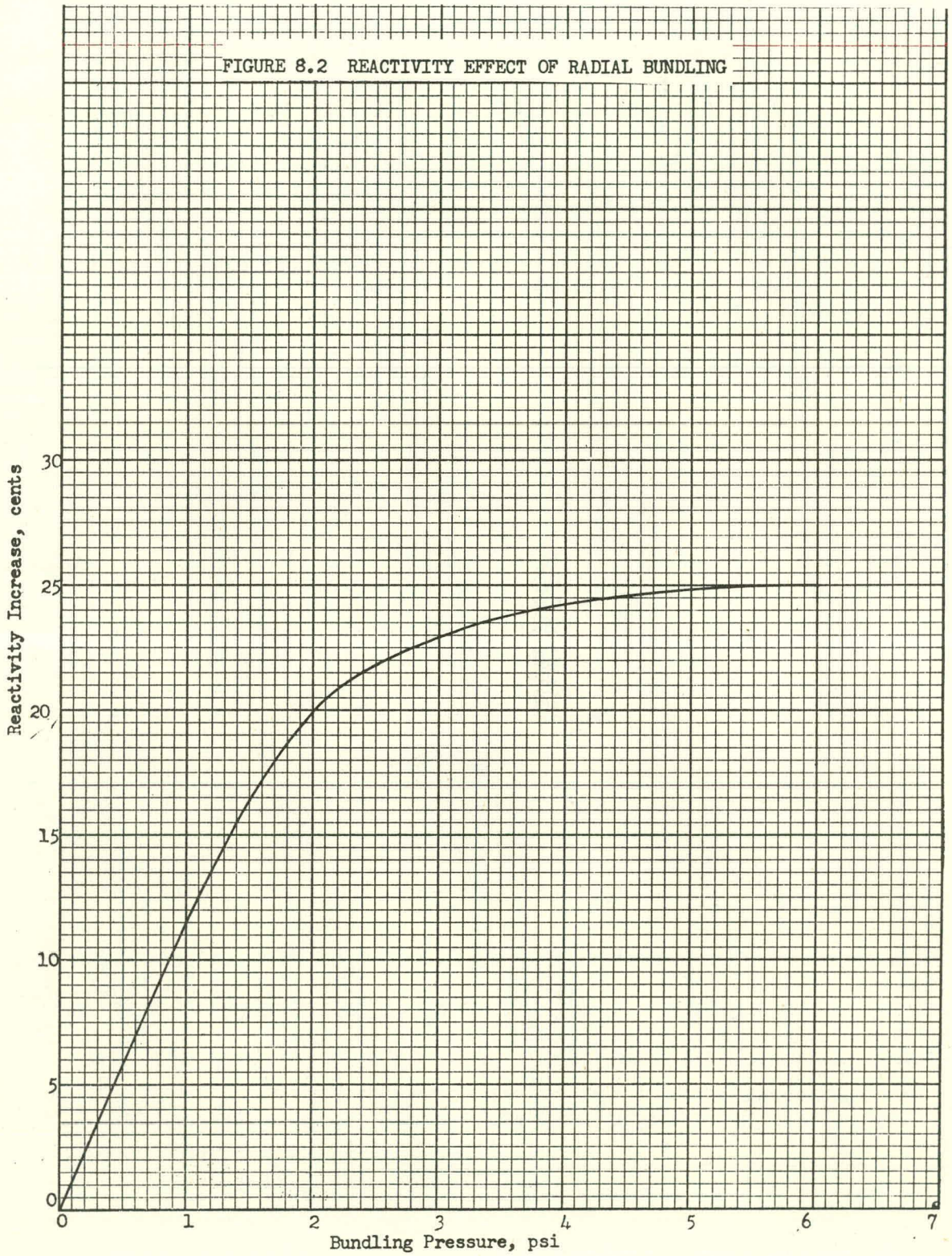

Since the pressure vessel is external to the reflector, the reactivity effect of the pressure vessel is primarily a function of the scattering cross section. Therefore, the worth of the NRX-A6 pressure vessel was taken to be the product of the experimentally measured reactivity effect for the PAX pressure vessel and ratio of the macroscopic scattering cross sections of the two pressure vessels. This calculation resulted in a net worth for the NRX-A6 pressure vessel of 0.33$.

SECTION 9.0

(CRD) UNCERTAINTIES IN THE NRX-A6 REACTIVITY ESTIMATE

As noted earlier, it was found that the 2 σ reactivity uncertainty due to mass uncertainties was $\pm$0.38\$, and the 2 σ reactivity uncertainty due to reactivity effect uncertainties was $\pm$0.58\$. The statistical sum of these uncertainties is $\pm$0.69\$, which is equivalent to $\pm$10° of control drum motion.

Figure 9.1 summarizes past experience in reactivity shimming previous NRX reactors. From this data, it was found that the average reactivity discrepancy in shimming previous NRX reactors was -0.35\$ with a 2 σ variation of 0.62\$. On the basis of this data, it was decided to shim the NRX-A6 reactor to a lower cold critical drum position in order to meet the aim drum angle of 88°. An added factor in determining this lower drum position was the possibility of violating the minimum shutdown requirement at the Test Site. Therefore, the NRX-A6 reactor shimmed to give a cold critical drum position of 85.2°. The reactivity estimate at that time was based on a core inventory which was not complete. The reactivity estimate based on the final core inventory(1) indicated that NRX-A6 should have a cold critical drum position of 87.4°.

If the uncertainty analysis derived in Sections 4.3 and 5.4 is used, the NRX-A6 reactor should have, to a 2 σ uncertainty, a cold critical drum position between 78° and 98°. However, if the uncertainty derived from previous NRX reactors is used, the NRX-A6 reactor should have, to a 2 σ

(1) The results presented in this report are based on the final inventory.

FIGURE 9.1

EXPERIENCE IN REACTIVITY

SHIMMING PREVIOUS NRX REACTORS

Reactor	Aim Drum Position, Degrees	Actual Drum Position, Degrees	Reactivity Discrepancy, Dollars
NRX-A2	90	97.8	-0.59
NRX-A3	90	89.1	0.07
NRX-A4	94	99.1	-0.38
NRX-A5	93	99.4	-0.48

Average Reactivity Discrepancy	-0.35$
One Standard Deviation(1) on the Discrepancy	0.31$

(1) $$\sigma = \sqrt{\frac{\sum_{i=1}^{N} (X_i - \bar{X})^2}{N-1}}$$

uncertainty, a cold critical drum position from 84° to 102°. From experience, the problems and experimental anomalies encountered in shimming the NRX-A6 reactor lead to the intuitive conclusion that the assignment of a 62¢ error to NRX-A6 is somewhat optimistic.

SECTION 10.0

(CRD) DETERMINATION OF THE NRX-A6 NEGATIVE SHIMMING

10.1 Selection of the NRX-A6 Aim Cold Critical Drum Position

Analysis of the expected corrosion behavior for the NRX-A6 fuel indicated that a hot start-of-life drum position of 90° and an orifice drum position of 105° would be desirable. Therefore, to determine the aim cold critical drum position of the NRX-A6, it is required that the cold-to-hot reactivity change of the NRX-A6 reactor in going to full power operation be determined.

The initial analysis of the NRX-A6 cold-to-hot reactivity change indicated a reactivity effect of -0.13$. However, the final analysis of the NRX-A6 cold-to-hot change, performed after the NRX-A6 had been shimmed, indicated a cold-to-hot reactivity loss of 0.03$. Based on the initial analysis of the cold-to-hot reactivity change, the aim cold critical drum angle of the NRX-A6 was chosen to be 88°.

Figure 10.1 shows in detail the components comprising the final analysis of the cold-to-hot reactivity change. The three components of this reactivity change are temperature effects, hydrogen effects, and loss of molybdenum coating during the startup. The net reactivity effect of each of these components is respectively-2.87$, +2.24$, and +0.60$. This results in a net reactivity change in going from ambient to full power operating conditions of-0.03$. This analysis indicates that if the NRX-A6 reactor goes critical at the predicted drum position of 87.4° the reactor will have a hot start-of-life drum position of 87.9°.

FIGURE 10.1

NRX-A6 OPERATING REACTIVITY CHANGES

Conditions	
Operating Power (100 Percent Power)	1120 MW Thermal
Propellant Flow Rate	71.3 lb/sec
Ambient Temperature	528°R
Cold-to-Hot Reactivity Changes (Determined by COHOT Calculation)	
Temperature Effects	
Due to core expansion	$ -1.61
Due to thermal base shift	-0.52
Due to Doppler effect - for U	-0.42
- for Nb	-0.26
- for Ta	-0.11
Due to Be contraction	+0.05
Subtotal of Temperature Effects	$ -2.87
Hydrogen Effects	
Due to core hydrogen	$ 1.64
Due to lateral support	0.09
Due to Be reflector	0.22
Due to change in worth of H_2 with temperature	0.07
Due to release of adsorbed H_2	0.00
Due to diffused hydrogen	0.22
Subtotal of Hydrogen Effects	$ 2.24
Net Change in Feedback Reactivity	$-0.63
Changes Due to Material Loss	
Loss of Molybdenum during startup	$ 0.60
Total Reactivity Change from Ambient to Full Power	$-0.03

10.2 Summary of the NRX-A6 and PAX-El Reactivity Comparison

Figure 10.2 shows the summary of the reactivity differences between the NRX-A6 and PAX-El reactors obtained in the preceding sections of this report. The sum of these reactivity differences indicates that the NRX-A6 is 0.02$ more reactive than the PAX-El reactor. Since the PAX-El reactor had an ambient delayed critical drum position of 87.7°, the NRX-A6 should have an ambient delayed critical drum position of 87.4°.

10.3 Selection of the NRX-A6 Shim Content

The distribution of the 38 TaC-loaded central support elements required to make the NRX-A6 critical at 87.4° is given in Figure 2.1. The distribution of the shimmed elements was chosen to be symmetrical in the azimuthal direction, and uniformly distributed over the regular cluster region of the core. In addition to meeting this criteria, the shim configuration had to meet the added constraints of the building schedule for the core and the exact negative reactivity requirements.

FIGURE 10.2

SUMMARY OF NRX-A6 AND PAX-E1 REACTIVITY DIFFERENCES

Core Reactivity Difference,	
NRX-A6 Minus PAX-E1, ¢	
Fueled Elements	115.7
Unfueled Elements	-194.6
Hardware	-36.1
Non-Core Reactivity Difference	
NRX-A6 Minus PAX-E1, ¢	
Subtotal A, Inventory Difference	78.5
Subtotal B, Instrumentation, Shield and Miscellaneous Differences	38.5
NRX-A6 Excess Reactivity at the PAX-E1 Ambient Delayed Critical Drum Position of 87.7°, ¢	2.0
NRX-A6 Ambient Delayed Critical Drum Position	87.4 degrees

(U) 11.0 REFERENCES

1. WANL-TME-1355, "NRX-A4/EST Reactivity Analysis with the Automated Materials Data System", January, 1966.

2. WANL-TME-1113, "NRX-A3 Reactivity and Shimming Report", March, 1965.

3. WANL-TME-878, "NRX-A2 Reactivity and Shimming", July, 1964.

4. WANL-TME-1642, "NRX-A6 Nuclear Subsystem, Thermal and Nuclear Design Data Book", November, 1967.

5. WANL-TNR-099, "Safety Report for the Westinghouse Astronuclear Experimental Facility (PAX and FCX)", January, 1967.

6. N-2-7166, "Los Alamos N-2 Group Progress Report", January, 1962.

~~CONFIDENTIAL~~
~~RESTRICTED DATA~~
~~Atomic Energy Act 1954~~

~~CONFIDENTIAL~~
~~RESTRICTED DATA~~
~~Atomic Energy Act 1954~~